Journal of Structural Geology 33 (2011) 255–270

Contents lists available at ScienceDirect

Journal of Structural Geology

journal homepage: www.elsevier.com/locate/jsg

Low-temperature deformation of limestone, Isola Palmaria, northern Apennine, Italy – The role of primary textures, precursory veins and intracrystalline deformation in localization

Giancarlo Molli [a], Joseph Clancy White [b,*], Lori Kennedy [c], Veronica Taini [a]

[a] Dipartimento di Scienze della Terra, Università di Pisa, Via Santa Maria, 56126 Pisa, Italy
[b] Department of Geology, University of New Brunswick, 2 Bailey Drive, Fredericton, NB E3B 5A3, Canada
[c] Department of Earth and Ocean Sciences, University of British Columbia, 6339 Stores Road, Vancouver, BC V6T 1Z4, Canada

ARTICLE INFO

Article history:
Received 1 January 2010
Received in revised form
9 November 2010
Accepted 23 November 2010
Available online 8 December 2010

Keywords:
Calcite
Localization
Rheology
Low-temperature deformation
TEM
Apennine orogen

ABSTRACT

Fine-grained limestones of the Tuscan nappe from Isola Palmaria (northern Apennine, Italy) contain sporadically developed, bedding-parallel shear zones, some of which exhibit well-developed calcite mylonites. The presence of shear zones that formed at temperatures less than 250 °C allows the study of limestone deformation mechanisms active under low-temperature, upper-crustal conditions. Two materially distinct types of shear zones developed during the syn-nappe stage of deformation and have been characterized by integrated field, strain, microstructural (optical microscopy, cathodoluminescence, transmission electron microscopy) and EBSD fabric studies. Type A shear zones occur within decametre-thick packages accommodating heterogeneously distributed strain in very fine-grained limestone (micrite). Type B shear zones are localized within calcite veins that develop into recrystallized calc-mylonites. Both types form at the contact with dolomite, although this does not play an important role in strain localization. In both cases, low-temperature ductility occurs by extensive dislocation glide sustained by athermal network-accommodated recovery. Although, the end-state microstructures of both shear zone types cannot be differentiated optically, differences do exist in the crystallographic preferred orientations (CPO) and the grain boundary structure of deformed micrite and vein calcite. Deformed micrite grain boundaries are rich in voids consistent with extensive fluid flux that can enhance material transport and independent grain displacements, while suppressing CPO development. The crystallographically defined grain boundaries in recrystallized vein calcite suggest that lower grain boundary diffusivity enables more typical dislocation-mediated CPO formation.

1. Introduction

Ductile localization within carbonate rocks is central to tectonic detachment within a host of geological regimes (Schmid, 1975; Linzer et al., 1995; Lickorish et al., 1996; Kennedy and Logan, 1997; Teixell et al., 2000; Thomas et al., 2002; Ulrich et al., 2002; Iannace and Vitale, 2004; McQuarrie, 2004; Spratt et al., 2004; Herwegh and Pfiffner, 2005; Behrmann and Tanner, 2006; Ebert et al., 2007a; Vitale et al., 2007 amongst others). Such localization is variously characterized as a consequence of parameters that include boundary conditions, temperature, pressure, differential stress, fluid activity, grain size and other material attributes. With the objective of further elucidating the deformation mechanisms of upper-crustal carbonates, shear zones have been examined on Isola Palmaria, in the northern Apennine of Italy (Fig. 1).

The study examines fine-grained carbonates and veins deformed at shallow crustal depths on the order of 7–9 km and temperatures of 200–250 °C. Although the shear zones are parallel to bedding, the boundary conditions induced by this mechanical anisotropy are apparently not in themselves sufficient to induce localization, as demonstrated by those rock volumes in which shear localization does not form. The question of "why localization here?" becomes equally one of "why no localization there?" The small grain size of the protolith and low temperature of deformation, coupled with the presence of fluids during deformation portend an important role for deformation mechanisms such as fracture and pressure solution or other grain-size-sensitive (GSS) processes (Rutter, 1974; Schmid, 1976; Kennedy and White, 2002 and references therein). Nevertheless,

* Corresponding author. Tel.: +1 506 447 3187; fax: +1 506 453 5055.
E-mail addresses: gmolli@dst.unipi.it (G. Molli), clancy@unb.ca (J.C. White), lkennedy@eos.ubc.ca (L. Kennedy).

0191-8141/$ – see front matter © 2011 Elsevier Ltd. All rights reserved.
doi:10.1016/j.jsg.2010.11.015

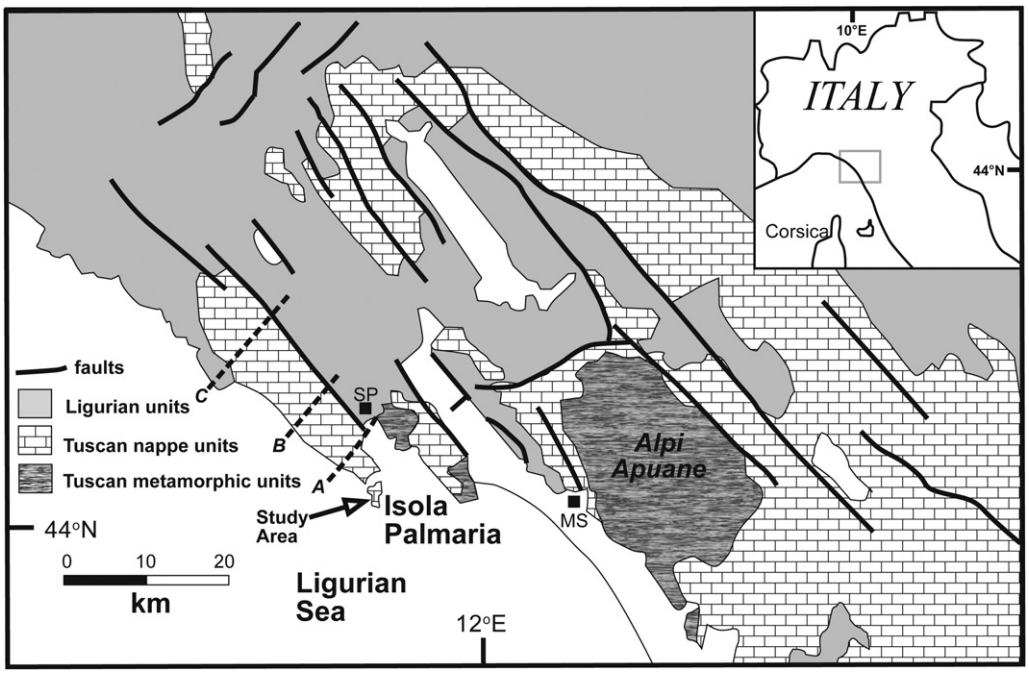

Fig. 1. Simplified geological map of the inner northern Apennine (see inset) with location of the study area on Isola Palmaria. Dashed lines are traces of cross-sections shown in Fig. 2. SP – La Spezia; MS – Massa.

well-developed shear zone fabrics and calc-mylonites indicative of plastic deformation are observed. The latter suggest that dislocation glide and dynamic recrystallization also play an important role in the deformation. Demonstration of such intracrystalline deformation would confirm scattered observations from naturally deformed limestone (e.g. Burkhard, 1990; Teixell et al., 2000; Badertscher and Burkhard, 2000; Kennedy and White, 2002) and attest the common occurrence of low-temperature crystal plasticity in calcite.

2. Geological setting

The shear zones in this study occur within Upper Triassic/early Liassic carbonates (Portoro beds) on Isola Palmaria at the southern termination of the La Spezia promontory, Italy (Fig. 1) within the inverted limb of the La Spezia fold (Fig. 2), part of the Tuscan nappe, a continent-derived unit of the northern Apennine nappe stack (Elter, 1960, 1975). The Portoro limestone forms part of the lowermost 100–200 m of the Tuscan nappe strata and is overlain by approximately 2000 m of younger units (Ciarapica and Passeri, 1980). Portoro is characterized by a fine-grained black matrix of calcite with alternating layers of mixed calcite and dolomite plus white carbonate veins, gold-coloured dolomite and limonite-rich stylolites. Two major pre-nappe dolomitization events that influence shear zone formation are recognized within the Portoro limestone (Miller, 1988; Miller and Folk, 1994).

Tuscan nappe units, including the Portoro limestone, were accreted at a shallow structural level in the northern Apennine orogenic wedge beginning in early Miocene (Federici and Raggi, 1976; Bernoulli, 2001; Cerrina Feroni et al., 2002; Molli and Vaselli, 2006). Burial occurred under a sequence of thrust sheets now represented in the overlying Canetolo and Ligurian units (Fig. 1). The shear zones of interest formed during thrusting as demonstrated by the asymmetry of shear foliations within different limbs of the fold (Gianmarino and Giglia, 1990; Taini, 2003). The nappe stack was subsequently modified by low-angle normal faults and related tectonic thinning (Carmignani et al., 1995; Storti, 1995;

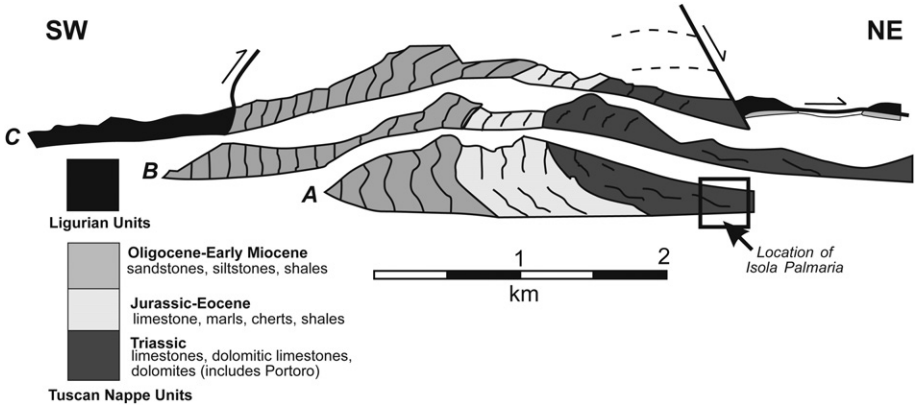

Fig. 2. Composite cross-section (from sections A, B, C of Fig. 1) across the western promontory of La Spezia. Note location of Isola Palmaria study area in the inverted limb of the kilometre-scale La Spezia fold.

Molli and Vaselli, 2006). The La Spezia backfold and overprinting upright folds and low-angle normal faults (Fig. 2) are related to later Miocene evolution of the northern Apennine wedge (Molli, 2008).

Metamorphism to anchizone grade (Cerrina Feroni et al., 1983) during burial and deformation has been tectono-stratigraphically constrained to a maximum depth of 7 km for the youngest nappe unit, Macigno sandstones (Reutter et al., 1978). Temperature estimates extrapolated to the burial depth of the Portoro limestone are summarized in Fig. 3.

3. Overview and methodology

Bedding-parallel shear zones in the Portoro beds were first described by Carter and Mosher (1987) and were subsequently studied by Carter (1990, 1992) and Carter and Dworkin (1990). In our study, two types of bedding-parallel shear zones are distinguished by their mesoscopic characteristics (Fig. 4). At the outcrop scale, both reflect some control by the mechanical anisotropy of contrasting micritic limestone and dolomitic layers. Nevertheless, these boundary conditions do not in themselves explain localized shearing in that outwardly equivalent exposures may or may not contain shear zones. Shear zone of both types have been examined with the aim of extracting the relationships among strain, microstructure, crystallographic texture and deformation mechanisms that contribute to localization.

Type A shear zones develop in arrays that form strata-parallel packages several metres thick. Individual shear zones 2–15 cm thick develop within the protolith micrite and are recognized by distorted bedding-perpendicular veins. Non-coaxial deformation dominates with near simple shear conditions being estimated (Carter, 1992; this study). Variation in shear strain can be calculated at different distances from the shear zone center (e.g. Ramsay, 1967) as

$$\gamma = \cot\gamma \cdot a - \cot\gamma \cdot a' \quad (1)$$

In Eq. (1), α and α' are, respectively, the angles between the shear zone boundary and undeflected/deflected veins, assuming the vein to be a passive strain marker. Bulk shear strain (γ) estimated by assuming passive vein reorientation ranges from 0.1 to 10. These are necessarily minimum values given the internal deformation of the vein; nevertheless, they provide constraints on the deformation gradient that are useful for comparing different areas. Type B bedding-parallel shear zones occur between metre-thick massive dolomites, and are singularly associated with vein-derived white calc-mylonites 5–30 cm thick. Shear strains can be very high, commonly exhibiting $\gamma > 10$.

Optical microstructures were determined from ultrathin sections (<5 mm thick). Grain size was analyzed by the GRAINSIZE method, while grain shape analysis utilized the SURFOR and PAROR programs (Panozzo Heilbronner, 1992; University of Basle, http://pages.unibas.ch/earth/micro/index.html). Crystallographic fabrics were determined by electron back-scattered diffraction (EBSD) using a Hitachi S-570 scanning electron microscope (SEM) and HKL Channel 5® software (University of British Columbia). Transmission electron microscopy (TEM) was carried out with a JEOL 1230 STEM operating at 200 keV on samples prepared by ion-beam thinning (University of New Brunswick). Crystallographic notation for calcite uses Miller–Bravais indices based on a hexagonal unit cell with $a = 0.499$ nm and $c = 1.706$ nm.

4. Shear zone development in Portoro limestone

4.1. Type A shear zone

The Type A shear zone (Fig. 5) examined (SZA) comprises an 8 cm thick deformation zone within micrite across which an initially bedding-perpendicular calcite vein is non-coaxially deformed. The maximum shear strain calculated within the shear zone using deformed markers (veins and fecal pellets) is $\gamma = 3.4$. Concomitant deformation of the vein and micrite enables comparison between initially coarse-grained vein calcite and the very fine-grained calcite at different strains. Three areas (Fig. 5a) of different shear strain defined by vein distortion ($\gamma 1 \cong 0 < \gamma 2 < \gamma 3 \cong 3.4$) were chosen for comparison of phenomena.

Initially coarse-grained vein calcite (Fig. 5b, area 1) exhibits an intracrystalline deformation sequence that progresses from undulose extinction, through twinning and twin boundary migration (Fig. 5c, area 2), to much smaller dynamically recrystallized grains (Fig. 5d, area 3). The end-state microstructure cannot be differentiated from the micrite, excepting a few grains that contain relict twins. Recrystallized grains (Fig. 6) are concentrated in the 5–10 μm range (75% < 10 μm).

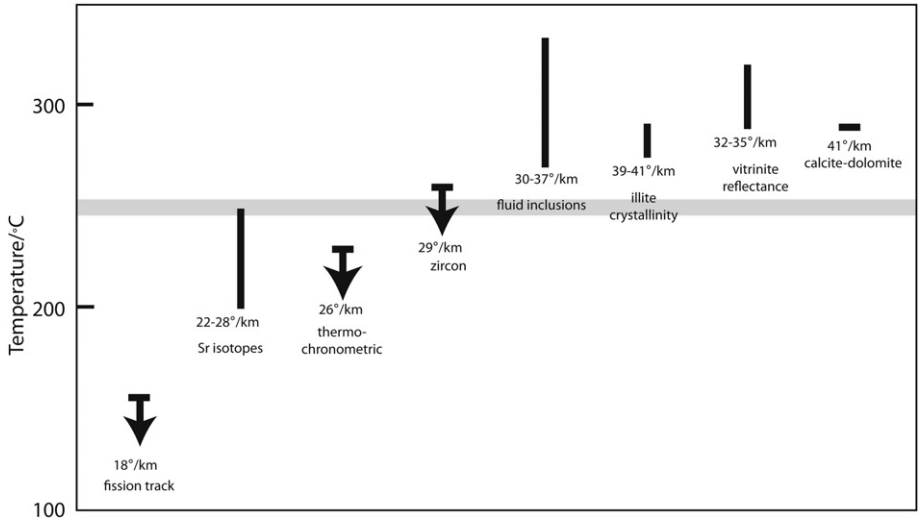

Fig. 3. Temperature estimates, re-calculated where necessary for the stratigraphic depth of the Portoro limestone, proposed by different authors for the Tuscan nappe in the studied area. Nominal geothermal gradients are calculated for each temperature. Data are from vitrinite reflectance (Reutter et al., 1978), stable isotopes (Carter and Dworkin, 1990), fission track on apatite (Abbate et al., 1994; Balestrieri et al., 2003; Zattin et al., 2002) and zircon (Bernet et al., 2004; Fellin et al., 2007), fluid inclusions (Montomoli et al., 2001; Montomoli, 2002), illite crystallinity (Cerrina Feroni et al., 1983; Carosi et al., 2003) and calcite-dolomite geothermometry (Carosi et al., 2003).

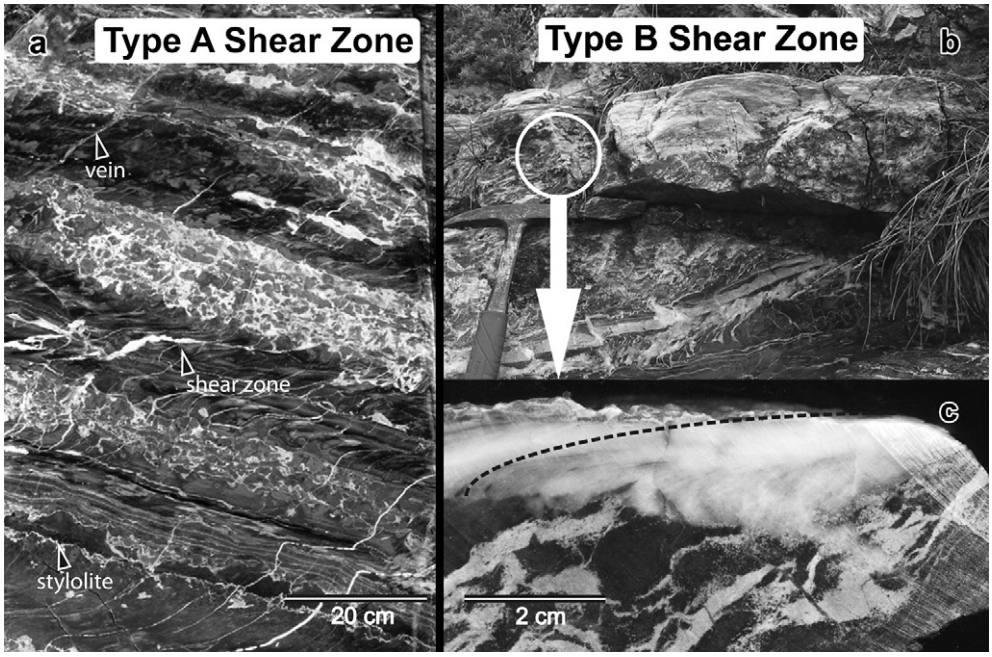

Fig. 4. Mesoscopic character of the two different types of bedding-parallel shear zones (Type A and Type B) observable in the Portoro limestone of Isola Palmaria. Both types of structures show top-to-northeast shearing (top-to-right).

Grain sizes of both undeformed and deformed micrite are concentrated in the 5–10 μm size fraction (Fig. 6). The undeformed micrite (Fig. 5, area 1) has 90% of grains <10 μm and a significantly larger fraction of the smallest grains (14% *vs.* 5% < 2.5 μm) compared to deformed micrite (Fig. 5, area 2) has 85% < 10 μm. The undeformed micrite comprises approximately equant, nearly randomly oriented grains with grain anisotropy of 0.73 and boundary anisotropy near 0.80 (Table 1). In contrast, deformed micrite has a prominent shape preferred orientation (SPO) with a grain anisotropy of 0.60 and boundary anisotropy of 0.61 (Table 1). The SPO foliation is oriented at 20° to the shear zone boundary (SZB) which matches well with the angle of 18° predicted as the finite extension direction for an ideal simple shear of $\gamma = 3.4$.

EBSD analysis of the protolith (Fig. 7, Micrite-area 1) shows a weak primary crystallographic preferred orientation (CPO) with c-axis maximum quasi-parallel to bedding in both macroscopically undeformed micrite and within the high strain core of the shear zone (Fig. 7, Micrite- area 3). No preferred orientations of $\{10\bar{1}4\}$ or $\{01\bar{1}2\}$ planes are observed within the micrite in either area. The calcite vein exhibits orientation peaks in the undeformed state (Fig. 7, Vein-area 1) that are reorganized in the fine-grained recrystallized vein material into a CPO with a *c*-axis maxima oriented at a high angle to the foliation plane (Fig. 7, Vein-Area 3) and strong peaks for $\{10\bar{1}4\}$ and $\{01\bar{1}2\}$ planes.

Transmission electron microscopy (TEM) shows a complex range of defect microstructures. Undeformed grains of the micrite protolith (Fig. 5, area 1) have low aspect ratios (Fig. 8a) and intragranular defect structures comprising variably organized networks of dislocations (Fig. 8b). Tight dislocation loops and/or dislocation walls produce cellular structures approximately 200 nm across. Grain boundaries consist of irregular segments across which localized elastic occur (Fig. 8c) and commonly contain voids (Fig. 8d). Deformed micrite grains (area 2 of Fig. 5) are elongate, consistent with the optical SPO, and have significant numbers of glissile dislocations (Fig. 8e,f). Grain boundaries are irregular and heavily decorated with voids and tubules (Fig. 8 f), plus pores at triple junctions.

Vein calcite TEM substructures evolve with increasing shear strain, in correspondence with the optical microstructure. Microtwins are only observed in the lowest-strain samples, and even here are but are only rarely observed (Fig. 9a). Wavy dislocations form at low strain with slip in both r$\{10\bar{1}4\}$ and f$\{01\bar{1}2\}$ planes (Fig. 9b). At higher dislocation densities, networks form by increasing dislocation interactions (Fig. 9c) and become organized dislocation walls defining a new cellular structure (Fig. 9d). Subgrain walls correspond with cells that are typically 200 nm across (Fig. 9d), similar to those of the undeformed micrite, but are formed during deformation. With increasing dislocation density and subwall organization, there is a corresponding development of recrystallized grains. Recrystallization occurs mainly by subgrain rotation, but can include grain boundary migration, with cuspate grain boundary segments encompassing 200 nm grains comparable in size to the cellular substructure (Fig. 9e). Except for subtle variations in grain boundary structure and dislocation substructure, recrystallized vein calcite and deformed micrite grains cannot be differentiated (compare Figs. 8e and 9e). Exceptions are rare strain-free new grains formed along grain boundaries (Fig. 9f)

4.2. Type B shear zones

The Type B shear zone (SZB) is part of a composite bedding-parallel zone on the order of 2 m thick that composed of discrete decimeter-thick white calc-mylonite between massive dolomite layers mixed with undeformed zones (Fig. 4b). The calc-mylonite (Fig. 4c) derives from calcite veins that are still evident undeformed at the margin of the shear zone (Fig. 10). A shear-induced foliation becomes progressively more parallel to the shear zone toward the higher strained core.

In contrast to SZA that develops from the fine-grained host, SZB form within initially coarse-grained vein calcite (Fig. 10a). Grains initially deform by twinning, with somewhat finer twins and higher twin densities at high strain. Twins coexist with optical subgrains. Twin boundary migration is observed early in the

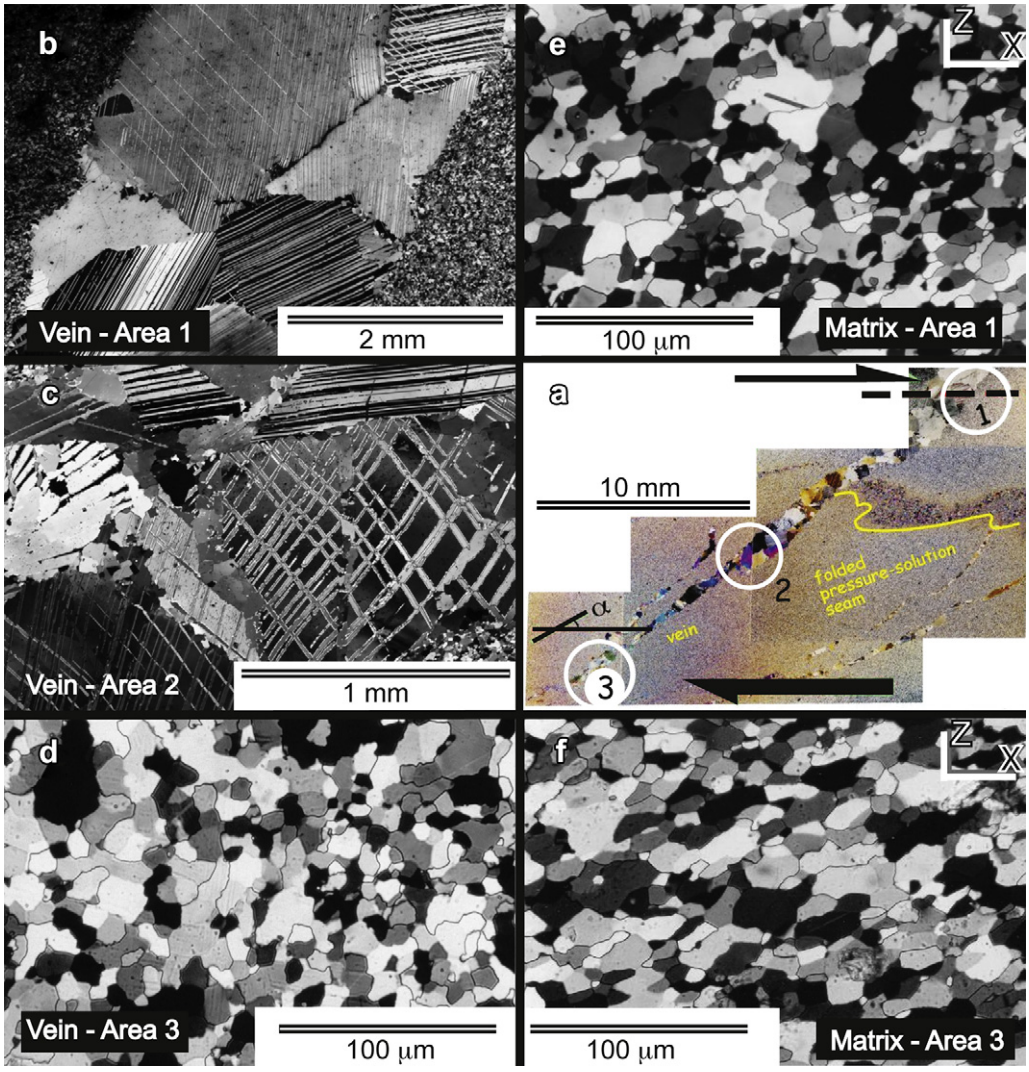

Fig. 5. Microstructural features of Type A shear zone. All photos are cross-polarized ultrathin sections (less then 5 μm) and XZ plane of the finite strain. (a) Overview of sample Type A shear zone with deformed calcite vein. Shear strain, defined by the angle α increases from area 1 to area 3. An early pressure solution seam, now folded, pre-dates the vein and shear zone. (b) Low-strain vein calcite with deformation largely restricted to twinning. (c) At higher strain, polysynthetic twins develop, along with twin migration to form blebby grains and optical bands. (d) Vein calcite at the highest strain is completely recrystallized, and generally indistinguishable from the host micrite. (e) Undeformed micrite (compare with 5d). (f) Highly deformed micrite displays a distinct shape preferred orientation (SPO) that defines the foliation.

deformation sequence, producing bleb-shaped deformation bands, many of which parallel the macroscopic slip plane (shear zone boundary). Localization of deformation along deformation bands creates calcite ribbons within a matrix of dynamically recrystallized grains (Fig. 10b). Reorientation of grains during deformation is seen in the progressive rotation of intragranular deformation bands toward parallelism with the macroscopic shear plane. In the shear zone core (Fig. 10c), no relict vein grains are observed and the recrystallized matrix has a marked concentration in the 3–5 μm grain size that is similar to that of the undeformed matrix (Table 1). The average aspect ratio of individual grains is 0.66 and bulk anisotropy ratio is 0.84.

A crystallographic preferred orientation (CPO) of calcite basal planes (0001) is present within undeformed portions of the calcite vein and increases in intensity with strain (Fig. 11). Development of the CPO is reflected in thin section by the progressive reorientation of deformation bands Fig. 10a. A well-defined *c*-axis maximum forms at a high angle to the foliation and is inclined to the shear zone boundary with quasi-monoclinic symmetry, consistent with the sinistral shear that is observed mesoscopically. The *c*-axis fabric maximum tends toward orthorhombic symmetry with respect to the shear planes toward the high strain shear zone core. Pole concentrations of $r\{10\bar{1}4\}$ and $f\{01\bar{1}2\}$ planes are initially absent and develop with strain to form intense maxima (Fig. 11).

Protolith micrite grains in SZB have TEM elements comparable to that of SZA (see Fig. 8); however, these are volumetrically minor as the bulk of the shear zone is dominated by vein calcite. The vein calcite grains exhibit a suite of TEM microstructures corresponding to increasing strain as demarcated in thin section by the change in orientation of the vein toward parallelism with the bedding/shear zone. Twins (e-type) form at low strain (Fig. 12a) with twin boundaries transforming at low strain into ordered dislocation arrays (Fig. 12b). In practice, few of the petrographically defined 'twin zones' are 'simple' or 'pure' twins, but rather slip bands and dislocation networks localized on pre-existing twins. Dislocation density develops heterogeneously within grains as these dislocation arrays develop into boundaries of new elongate grains (Fig. 12c). The elongate grains evolve to smaller, more equant grains (Fig. 12d) by a process of progressive misorientation (Fig. 12e). In

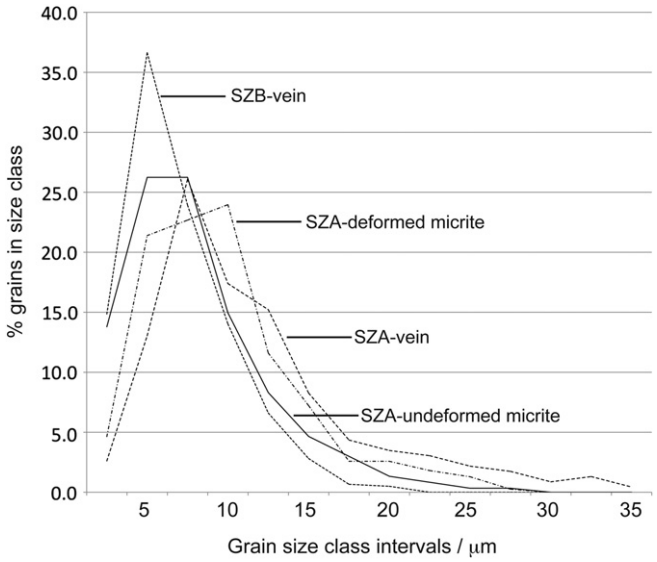

Fig. 6. Grain size distribution from different material elements of SZA and SZB plotted using data acquired using GRAINSIZE (Panozzo Heilbronner, 1992; University of Basel, http://pages.unibas.ch/earth/micro/index.html). Population fractions are plotted with respect to grain size classes, in increments of 2.5 μm.

comparison to SZA, calcite grain boundaries in SZB (Fig. 12f) are bereft of voids, precipitates or nanoparticles.

5. Discussion

5.1. Palmaria shear zone deformation – summary

The combination of similarities and differences between the shear zones from Palmaria reflects the range of micromechanical processes that accommodate calcite deformation within the same deformation environment. The similar timing and spatial proximity of SZA and SZB limit the variation in intensive parameters (e.g. temperature, pressure). Mesoscopic deformation is heterogeneous on the decimeter to metre scale. Although there is a first-order control by the mechanical anisotropy of the original multilayer on formation of bedding-parallel shear zones, it is insufficient to explain the localization. SZA forms mixed with otherwise identical, but undeformed micrite, and although SZB is bounded by bedding layers, not all such cases develop into shear zones. There is also the question as to why micritic limestone, a relatively strong material, though weak compared to dolomite, would deform ductily at low temperatures, let alone accumulate large macroscopic strains.

The contrasting nature of the calcite polycrystals must be considered in addressing localization – SZA localizes within the primary fine-grained micritic calcite, while SZB nucleated in very coarse-grained vein calcite. At high strain, the microstructures of both shear zones cannot be optically differentiated, although the evolution paths are distinct for each. Both show foliations (SPO) and similar dislocation defect structures, yet CPOs indicative of dislocation activity are distinctly different.

Table 1
Morphometric data for micritic and vein calcite from Type A (SZA) and Type B (SZB) shear zones.

	SZA UNDEF	SZA DEF	SZA DEF Vein	SZB DEF Vein
Harmonic mean grain size	5.9 μm	7.4 μm	8.8 μm	4.0 μm
Median grain size	7.5 μm	10.0 μm	10.0 μm	6.3 μm
Standard deviation	4.5	4.4	6.4	4.5
Grain anisotropy (PAROR)	0.73	0.60	0.66	0.66
Boundary anisotropy (PAROR)	0.80	0.61	0.83	0.84
Grain orientation (SUFROR)	~ random	~20° CW to SZB	~40° CW to SZB	~40° CW to SZB

5.2. Deformation mechanisms and microstructure evolution

5.2.1. Low-temperature crystal plasticity and athermal recovery

Postponing for the moment discussion of shear zone initiation, it is clear that once formed, crystal plasticity contributes significantly to the high-strain deformation of micrite and vein calcite in both shear zone types without evidence for thermal recovery typical of dislocation creep. Alternative recovery (strain energy reduction) processes must be invoked to accommodate the substantive ductile flow. The observed glide on $r\{10\bar{1}4\}$ and $f\{01\bar{1}2\}$ slip systems is typical of low-temperature dislocation activity in calcite (Turner et al., 1954; Wenk, 1985; de Bresser and Spiers, 1993). Importantly, cross-slip on the r- and f-systems can serve to overcome barriers to glide through movement of screw dislocations onto symmetrically related glide planes with the same Burgers vector (de Bresser, 2002). Athermal recovery sufficient to accommodate the intracrystalline deformation comprises cross-slip combines with interaction of these glide dislocations to form networks and cell walls (Figs. 8, 9 and 12). SZB calc-mylonite best expresses these textures with twin boundaries serving to concentrate/impede dislocation glide. The resulting dislocation interactions produce networks that define elongate cells and deformation bands quasi-parallel to e-twin orientations. Cell walls are in essence active or relict slip bands approximately parallel to the macroscopic shear plane. Such network-accommodated recovery has been recognized in both experimental and natural (de Bresser et al., 2002; Kennedy and White, 2002) low-temperature calcite deformation. Significantly, large strains are achieved in a glide-dominated regime without recourse to thermally controlled processes of recovery that are associated with dislocation creep flow laws.

5.2.2. Dynamic recrystallization and grain size evolution

Dynamic recrystallization of deformed vein calcite in both types of shear zones provides the potential to assess stress from its inverse relationship to dynamically recrystallized grain size (Twiss, 1977; Schmid et al., 1980; Urai et al., 1986; Rutter, 1995; de Bresser et al., 1998; Stipp and Tullis, 2003 amongst others). Grain size of a deformed aggregate will reflect the overall deformation history including temperature or strain rate (Guillopé and Porier, 1979; White, 1982; de Bresser et al., 1998; Herwegh et al., 2005a,b), the mechanism by which recrystallization occurs (Guillopé and Porier, 1979; White, 1982; Hirth and Tullis, 1992) and finite strain (Rutter, 1995, 1999; Kennedy and White, 2002). Austin and Evans (2007) have integrated many of these factors into an energy balance reflecting the rate of mechanical work whereby grain size is not a function of stress alone.

The grain size distributions (Fig. 6) represent to two end-member conditions: (1) the undeformed micrite host, which serves as a base state against which to compare deformed material and (2) the deformation end-state, expressed by all other grain size data, with only vein calcite grain size reflecting recrystallization. The mean grain sizes of all areas analyzed lie within a standard deviation of each other (Table 1) and could be interpreted as equivalent. Nevertheless, grain size evolution is subtly different for the two shear zone types. In both shear zones, vein calcite shows a reduction in mean grain size (Table 1) giving a resultant size distribution (Fig. 6) similar to that of the undeformed micrite. In contrast, the deformed micrite grain size distribution is broader relative to the undeformed material (Fig. 6) and has a larger mean grain size (Table 1).

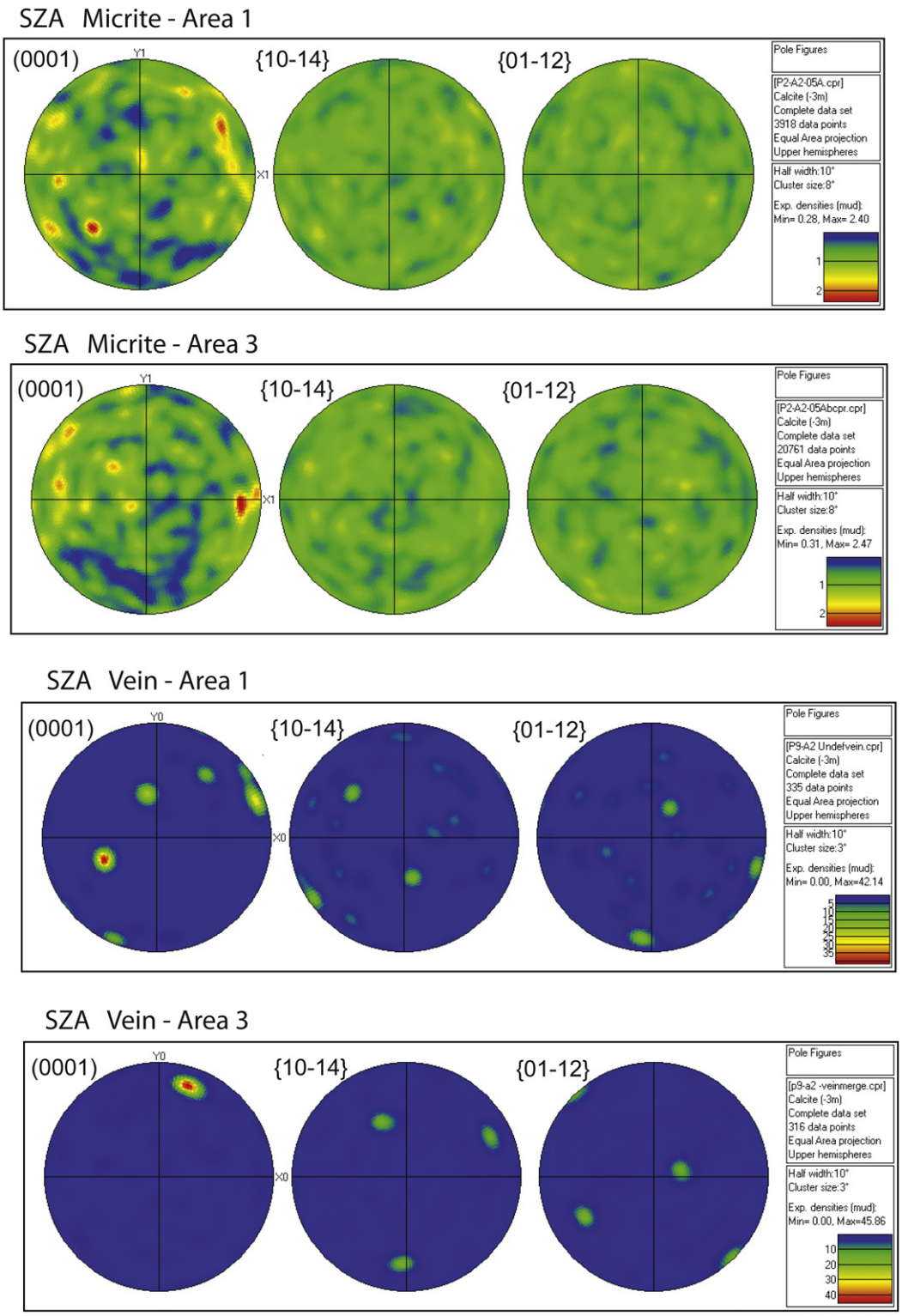

Fig. 7. ESBD patterns from the Type A shear zone. Poles to crystal planes are plotted on equal area, upper hemisphere. Contours of pole figures are an exponential scale displayed by the colour code. Note the different cluster size used for micrite (8°) and vein calcite (3°) contouring. This difference does not affect conclusions regarding CPO development. Details of the patterns are described in Section 4.1.

The equilibrium grain size in each case reflects the competition between rates of grain growth and grain size reduction. The latter is predicted by theory and has been observed in naturally deformed limestone (de Bresser et al., 1998; Herwegh et al., 2005a; Austin and Evans, 2007; Ebert et al., 2007b,c; and reference therein). Grain growth (boundary migration) in the micrite would be consistent with the protolith grains being smaller than the "stable" size dictated by dislocation-mediated dynamic recrystallization at the ambient deformation conditions; hence, the initially fine-grained material readjusts to a larger mean size during deformation, while the coarser vein calcite undergoes only grain size reduction. Similar microstructures have been observed for quartz where quartzite exhibits dislocation-mediated

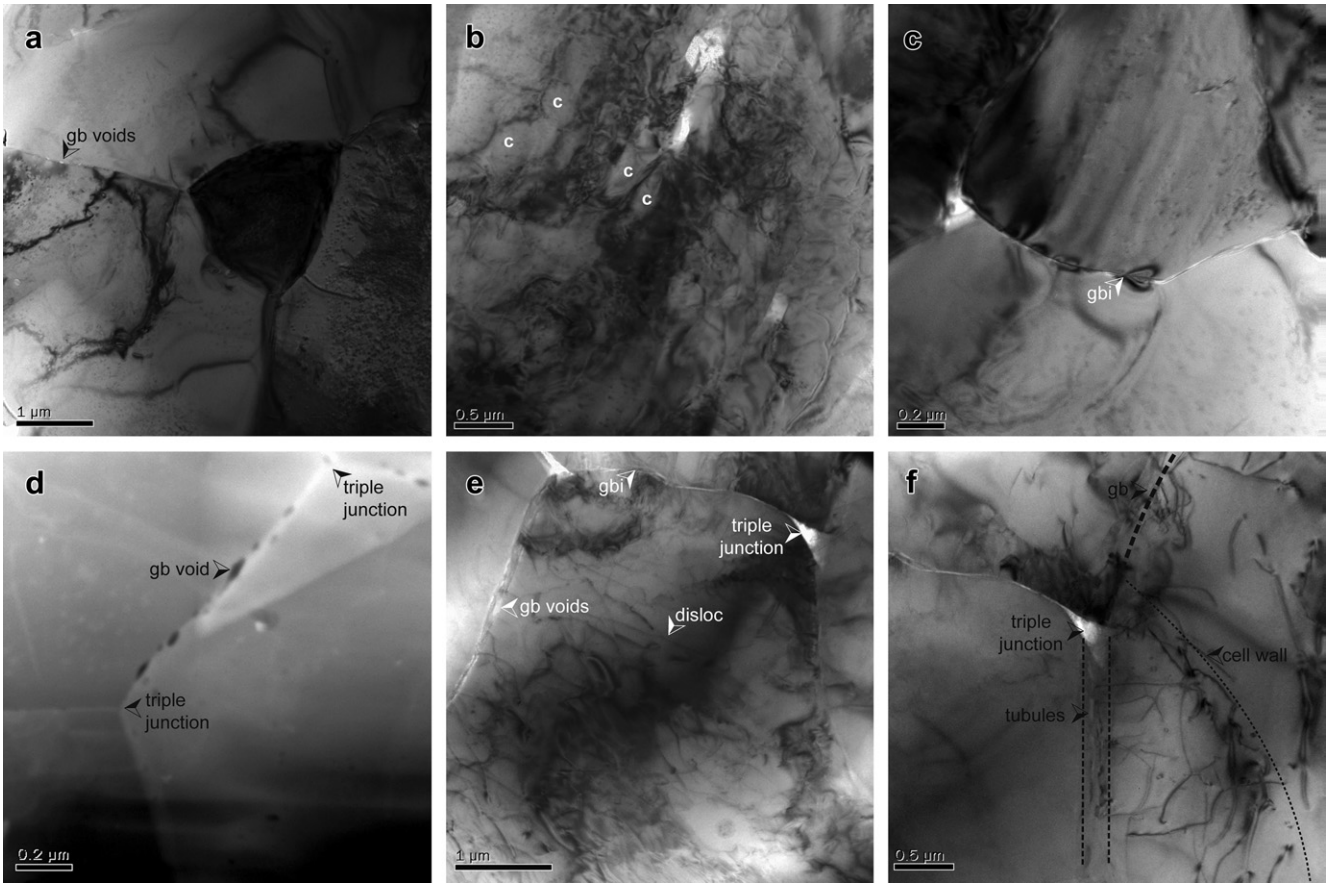

Fig. 8. Transmission electron microscopy of micrite from Type A shear zone. Bright field images except where noted. (a) Primary, undeformed micrite exhibiting the very small, equant grains typical of this calcite aggregate with grain boundary voids. (b) Intracrystalline defect texture of primary micrite grains comprising cells, c, on the order of 200 nm. (c) Elastic distortions and voids along grain boundaries. (d) DF image of equant grains with triple junction voids and grain boundary voids. (e) Deformed micrite grain with high density of dislocations. (f) Deformed micrite with void-rich grain boundary zones and dislocations. Cell structures form adjacent to grain boundaries.

grain size reduction, while chert (fine-grained quartz) displays grain growth toward the recrystallized grain size (White, 1982).

The fact that both mean grain sizes are smaller (Table 1) and the distribution is heavily concentrated at the small grain size classes (Fig. 6) suggests higher stress for SZB that SZA (Rutter, 1995) or alternatively, greater power dissipation (Austin and Evans, 2007). Despite the latter difference, the pre-existing micrite grain size appears to buffer the degree of grain size reduction by recrystallization in both shear zones; that is, the stable recrystallized grain size is approximately that of the micrite protolith.

5.2.3. *Grain boundaries, fluids and fabrics*

The material difference between the shear zone types, other than initial grain size, is most evident along grain boundaries. Grain boundary structure plays a fundamental role in deformation of tectonites (White and White, 1980; White, 1982; Mainprice and Paterson, 1984; McLaren, 1986; Herwegh and Kunze, 2002; Mancktelow et al., 1998; Mancktelow and Pennacchioni, 2004, amongst others). SZA micrite grain boundaries (Fig. 8) abound with inclusions and tubules indicative of fluid activity. Explicit evidence for fluid flux is provided by the geochemical analyses of Carter and Dworkin (1992) that documented preferential and extreme depletion of Sr within the shear zones relative to unsheared Portoro. Additionally, the cathodoluminescence signatures in recrystallized vein calcite observed by Taini (2003) correlates with localized syndeformational fluid interaction. Localized variations in fluid flux of this type are common in limestone-associated fault and shear zones (Kennedy and Logan, 1997; Kirschner and Kennedy, 2001) with direct impact on the mechanical response. In contrast, vein calcite grains from SZB have ‘clean, tight’, crystallographically defined grain boundaries (Fig. 12) and minimal evidence of fluid transport or interaction.

Grain boundary structure affects the mechanical response by the enhancement or suppression of material transport (Mistler and Coble, 1974; White and White, 1980, 1981; Pennock et al., 2009); hence, it is argued that SZA micrite has accommodated significant fluid flux through a larger defect volume along grain boundaries compared to the SZB grain boundaries. Enhanced diffusion zones of 30–100 nm width along grain boundaries (Fig. 8) would increase uniform strain rates by up to 100×, while easing the accommodation of grain boundary misfit to generate an additional strain rate component by independent grain boundary sliding (GBS).

The absence of a CPO in SZA micrite despite having an SPO fabric and extensive intracrystalline deformation can be reconciled if there is a significant contribution to strain by GBS. The latter combination of contradictory observations argues for independent grain boundary displacements aided by “relaxed” grain boundaries that counter the crystallographic co-ordination of grains during glide that will be. SZB grains, in contrast, more strictly define an ideal calcite polycrystal in which a CPO develops as anticipated during dislocation glide. A similar relationship between CPOs has been reported by Herwegh and Ebert (2009), but for calcite deformed at different temperatures; the lower temperature fine-grained material deformation has no CPO, while higher temperature, coarser calcite does. They

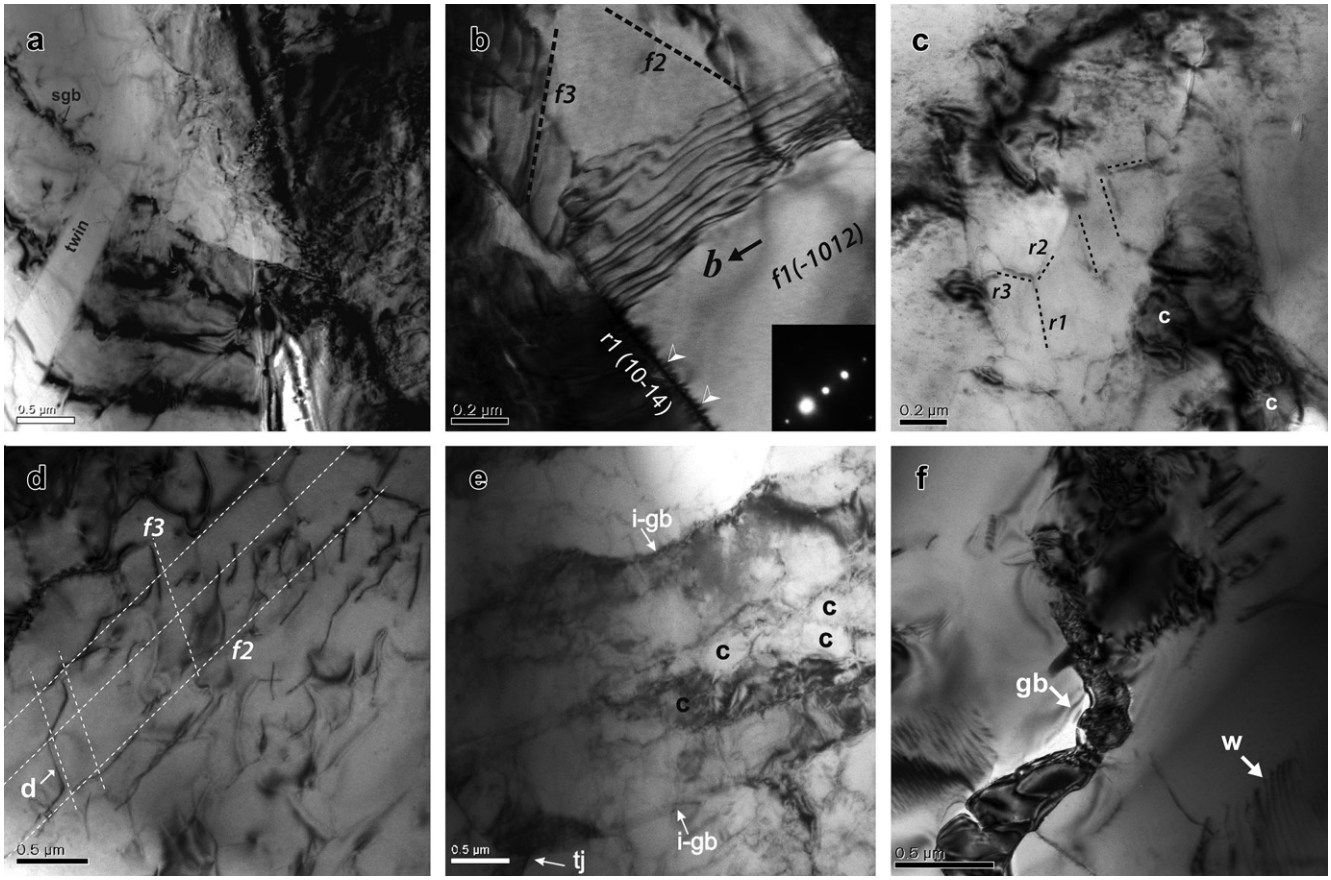

Fig. 9. Transmission electron microscopy of vein calcite from Type A shear zone. Bright field images except where noted. (a) Twin in low strain area. (b) Glide dislocations. The image plane is close to $f1(10\bar{1}4)$ glide plane in which wavy dislocations with long segments parallel the burgers vector, *b*. The traces of *f2* and *f3* planes have dislocations imaged parallel to them. The $r1(10\bar{1}4)$ and f slip plane is vertical, in which end-on dislocations are imaged (arrows). B = $[\bar{2}021]$ (c) Quasi-hexagonal networks of dislocations imaged along traces of $r\{10\bar{1}4\}$ planes, adjacent to cells, c. (d) Image plane is close to $f1(\bar{1}012)$ glide plane and is intersected by *f2* slip bands containing arrays of dislocations. Some dislocations have segments common to image plane and traces of the intersecting *f*-planes, consistent with cross-slip. (e) Elongate grains defined by cuspate, intermediary stage grain boundaries, i-gb, surrounding defect-rich cell structure, c. (f) New (crystallizing?), relatively strain-free grains formed along grain boundary, gb. These grains may originate in association with fluid flux, as they are atypical of the dominant rotation recrystallization texture. Dislocation walls, w, are developed in adjacent grains.

document the propensity for veining (and hence fluid flow) in the lower temperature, fine-grained flow regime comparable to the observations made in this study. However, in the Palmaria case, deformation was at the same temperature and the fundamental material difference affecting fluid flux is the grain boundary structure.

The apparent increase in grain size of the deformed SZA micrite relative to the undeformed material (Fig. 6) could also reflect grain growth kinetically enhanced by the fluids. Again, in contrast to this behaviour, SZB recrystallized calcite achieves a grain size more comparable to the undeformed micrite because any growth is suppressed by the slower grain boundary diffusivity.

5.3. Correlation of natural deformation with flow laws

5.3.1. Flow laws for natural deformation of calcite

Several factors enter into the choice of flow laws: (i) The prevalence of dislocation glide in the calcite supports use of glide-controlled relationships (Kocks et al., 1975), both cross-slip (de Bresser, 2002) and Peierls law type (Renner et al., 2002); (ii) the important role of rotation recrystallization requires incorporation of experimental results that exhibit this behaviour (Walker et al., 1990); (iii) the small initial grain size of the host micrite, plus the final grain size distribution of the recrystallized veins merit consideration of grain-size-sensitive (GSS) flow laws developed for comparable calcite aggregates (Walker et al., 1990; Herwegh et al., 2003).

The evidence for extensive dislocation glide supports arguments that calcite did not deform according to a power law relationship of the type

$$\dot{\epsilon} = A\exp(-Q/RT)\sigma^n \tag{2}$$

(see Appendix for parameters), but rather is controlled by the efficacy of dislocation glide. Cross-slip on the r- and f-systems, as observed in these shear zones, can act as a recovery process (de Bresser, 2002). Similarly, a Peierls law relationship (Renner et al., 2002) is consistent with the microstructural observations and incorporates a Hall-Petch type strength dependence on inverse grain size that is typical of low-temperature calcite deformation. The occurrence of glide-mediated low-temperature deformation at the inferred conditions is further supported by the experiments of Covey-Crump (1994) that demonstrated a transition from a deformation rate controlled by dislocation glide to one controlled by thermally activated processes (e.g. climb) at or below 250 °C.

The flow laws used to extrapolate experiments to the natural deformation are:

Cross-slip-controlled (de Bresser, 2002)

$$\dot{\epsilon} = K\left(\frac{\sigma}{\mu}\right)^2 \exp\left[\frac{\Delta U_{CS}\left(1-\frac{\alpha b\sigma}{\gamma}\right)}{kT}\right] \tag{3}$$

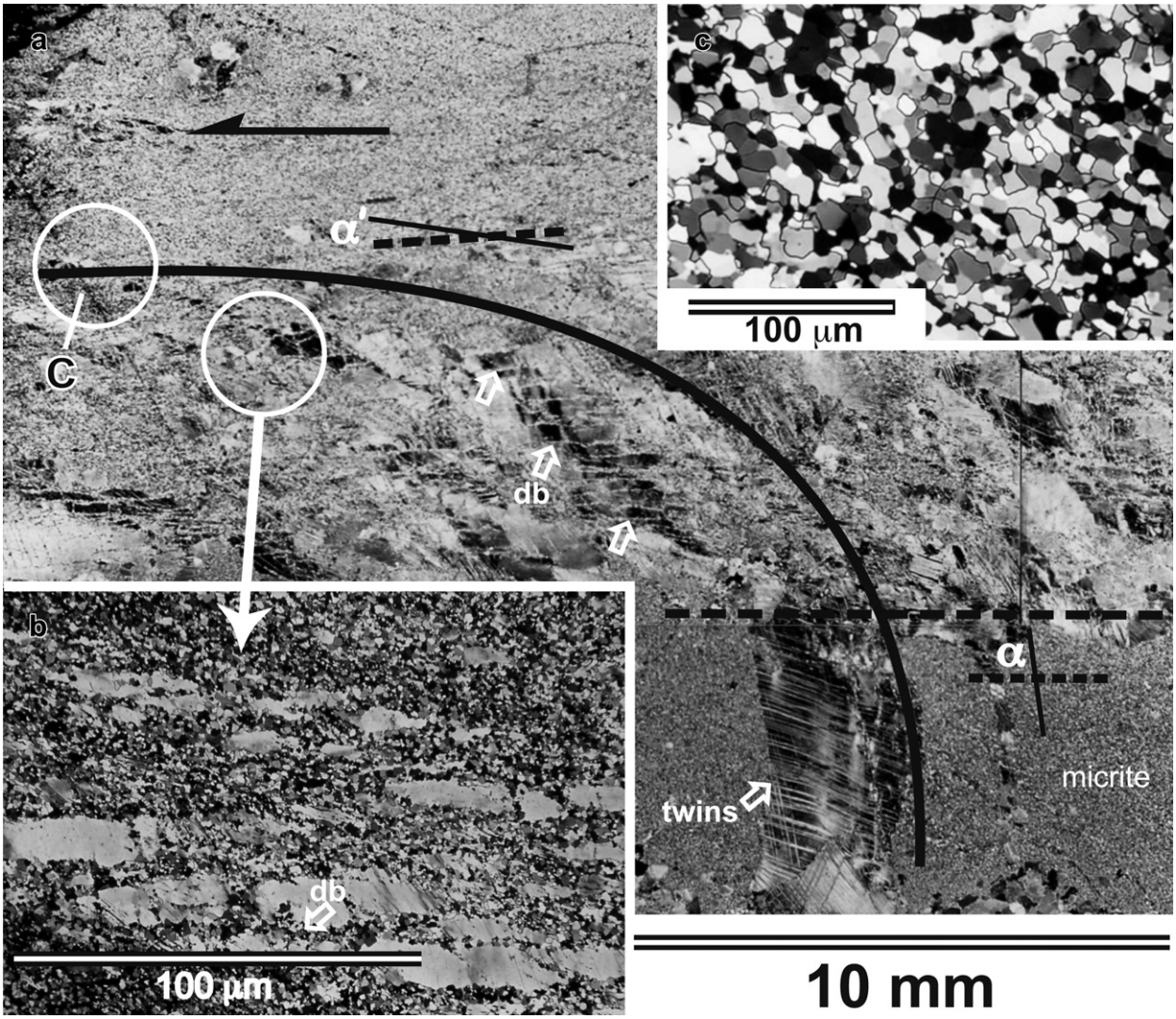

Fig. 10. Microstructural features of Type B shear zone. All images are cross-polarized from ultrathin sections (≤5 μm thick) and in the XZ plane of finite strain. (a) Overview of coarse-grained calcite vein in protolith micrite deformed (sinistrally in this image) into SZB. The shear zone slip plane (dashed lines) and vein orientation (solid line) are used to calculate changes in strain during deformation (see Eq. (1)). Twins form early in the deformation history, succeeded by localization of deformation bands (db) and recrystallized grains along relict twins and parallel to the macroscopic slip plane. (b) Dynamic recrystallization produces relict ribbon grains bounded by deformation bands, db, in a matrix of much finer grains. (c) Complete recrystallization in the shear zone core produces a microstructure that is optically the same as micrite (see Fig. 5).

Peierls stress-controlled (Renner et al., 2002)

$$\dot{\epsilon}_P = A_P \sigma^2 \exp\left(\frac{\sigma}{\sigma_P}\right) \exp\left(\frac{-Q_P}{RT}\right) \tag{4}$$

Power law (Walker et al., 1990)

$$\dot{\epsilon}_{GSI} = A_{GSI} \sigma^n d^m \exp\left(\frac{-Q_{GSI}}{RT}\right) \tag{5}$$

GSS dislocation-accommodated (Walker et al., 1990)

$$\dot{\epsilon}_{GSS} = A_{GSS} \sigma^n d^m \exp\left(\frac{-Q_{GSS}}{RT}\right) \tag{6}$$

GSS diffusion-accommodated (Herwegh et al., 2003)

$$\dot{\epsilon}_D = A_D \sigma^n d^m \exp\left(\frac{-Q_D}{RT}\right) \tag{7}$$

Values of the various parameters are given in the Appendix.

The flow laws that correspond to dislocation-dominated processes (Eq. (3)–(5)) differ by being either insensitive (cross-slip control) or weakly sensitive (Peierls law and power law relationships) to grain size. The power law relationship (Eq. (5)) incorporates an explicit grain size dependence determined by regression of experimental data (Walker et al., 1990), while the grain size dependence for Eq. (4) enters the relationship through calculation of the Peierls stress. Both of the latter differ from classic GSS relationships in that there is no dependence on grain boundary diffusion as in Eq. (7). Likewise, the GSS flow law expressed by Eq. (6) (Walker et al., 1990) does not explicitly invoke diffusion, nor do the stress exponent and grain size dependences correspond to classical grain boundary sliding (GBS) parameters (i.e. $n = 1$, $m = -3$); instead, the relationship is closer to the form proposed by Gifkins (1976) for dislocation-accommodated GBS. Consideration of both these GSS flow laws allows comparison of diffusion and dislocation accommodation of macroscopic flow at these crustal conditions; the latter is deemed important given the absence of thermally controlled (diffusion) microstructures. The particular flow laws chosen, as well as being deemed

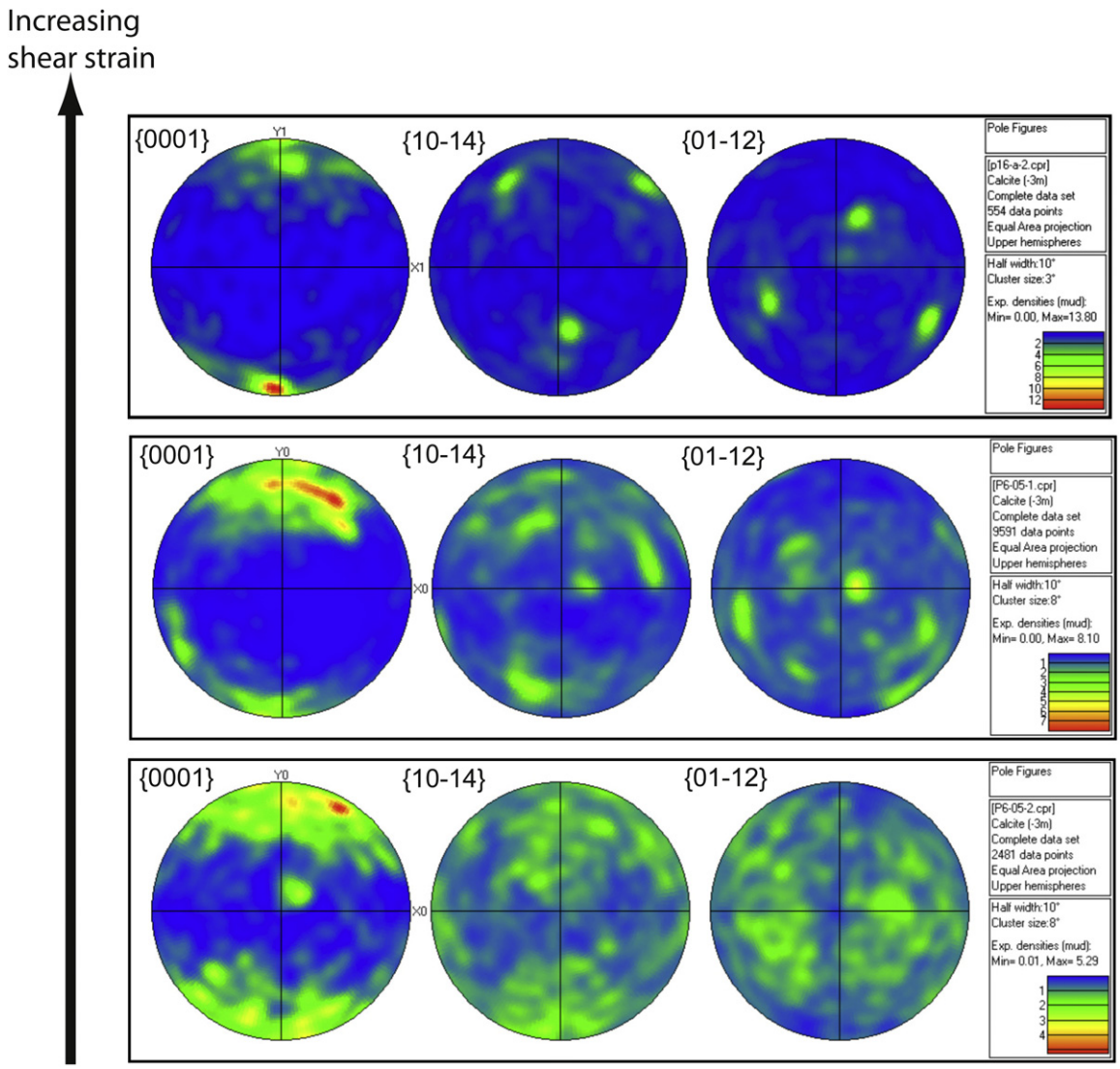

Fig. 11. ESBD patterns from the Type B shear zone. Samples increase in strain from top to bottom. Poles to crystal planes are plotted on equal area, upper hemisphere. Contours of pole figures are an exponential scale displayed by the colour code. Note that density cluster size is 8° for low and moderate strains, and 3° for the highest strain sample. This difference does not affect conclusions regarding CPO development. Details of the patterns are described in Section 4.2.

appropriate to this study, enable comparison to recent examinations of naturally deformed limestone (e.g. Herwegh et al., 2005b; Vitale et al., 2007).

5.3.2. Stress estimates

Two empirical paleopiezometric approaches are used to constrain stresses during deformation: (1) limits indicated by mechanical twinning and (2) stress ranges determined from recrystallized grain sizes. Calibration of twinning and stress in calcite integrates grain size effects, twin density and the relative volume of twinned material (Rowe and Rutter, 1990; Burkhard, 1992). Three calibrations for twinning stresses are used: (*I*) the first describes the effect of grain size and twin incidence in grains of a given size class (Eq. (1), Rowe and Rutter, 1990); (*II*) the second relationship incorporates grain size and the volumetric fraction of twinned material (Eq. (5), Rowe and Rutter, 1990) and (*III*) the final calibration is based on twin density and is independent of grain size (Eq. (2), Rowe and Rutter, 1990). SZB has both the largest initial grain size, and most intensely twinned grains. Because the twins are reorganized by subsequent glide and subwall formation, it is difficult to define unaltered twin densities and twinned volumes, though limits can be established from limited unaltered microstructures. For example, larger grains are the most susceptible to twinning (Turner, 1953; Schmid et al., 1977) and should record lower stresses. To represent this initial twinning prior to formation of dislocation substructures, a twinning incidence, I_t, and twinned volume, V, of 10% are used for 1 mm grains in SZB. These parameters correspond to a stress of 83 MPa using calibration (*II*), while calibration (*I*) is not applicable to this grain size. For the case of complete twinning where I_t and V are set at 100%, the upper end stress estimates are 124 MPa and 208 MPa for calibrations (*I*) and (*II*). The smallest grains have no twins, and rare twins in recrystallized vein calcite are suspected to be relicts of larger grains. Consistent with these observations are the stress estimates of 208 MPa from calibration (*I*) for $V = 10\%$ in 100 μm grains and $V = 1\%$ in 10 μm grains; that is, the maximum stress associated with the weakest grains is equivalent to the stresses needed to produce fewer twins in finer-grained material. A stress range of 97–150 MPa derives from calibration (*III*) based on a limited number of twin density measurements. These moderate stresses are consistent

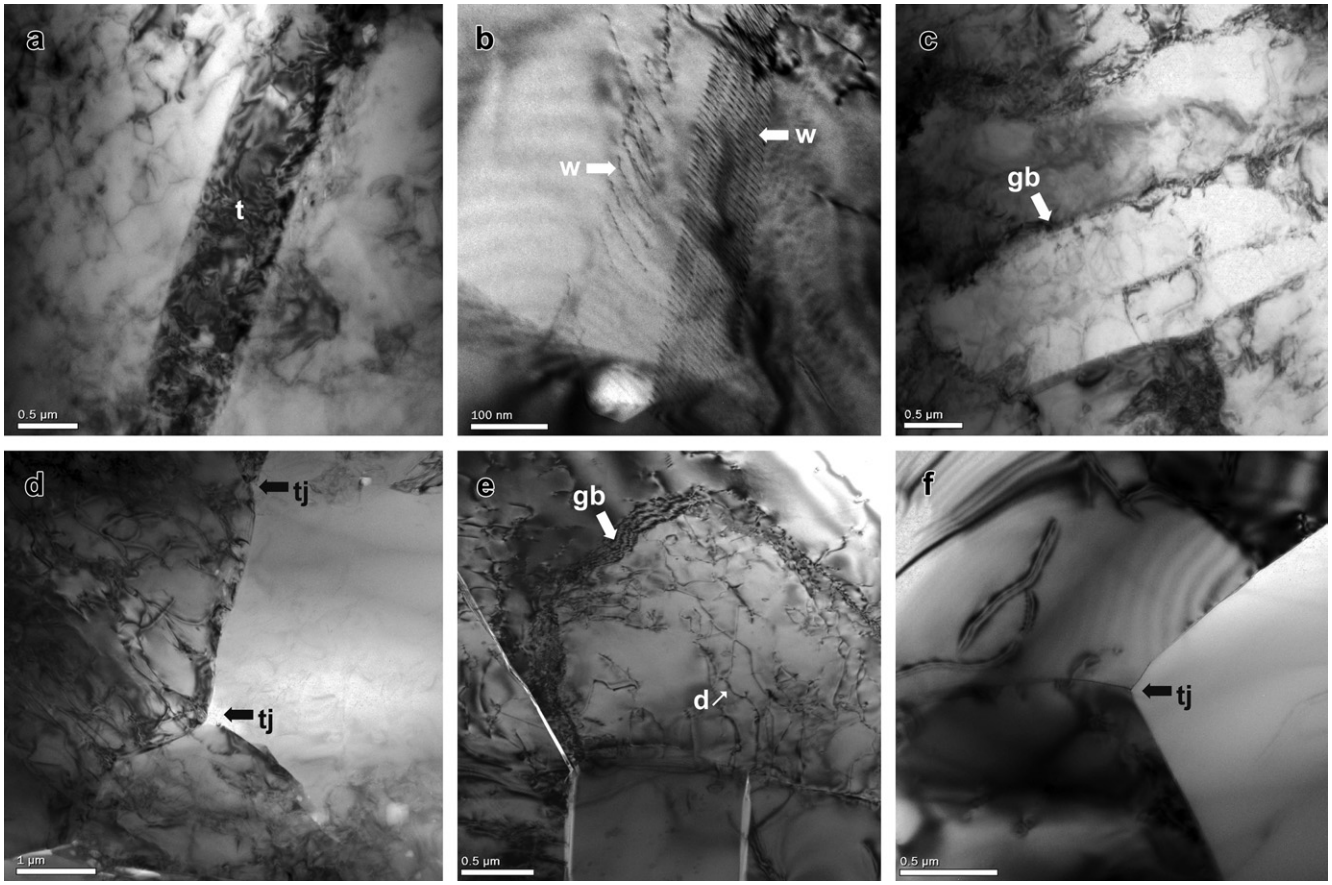

Fig. 12. Transmission electron microscopy of vein calcite from Type B shear zone. Bright field images except where noted. (a) Twin, *t*, in from relatively low strain area. The 'twin' exhibits a cellular defect structure within a dislocated host. (b) Twin oriented to image bounding dislocation walls. Twins act as accumulation sites for dislocations and are precursors to deformation bands. (c) Elongate grains formed by misorientation along dislocation networks to form new grain boundaries, gb. Collectively these grains define the slip-parallel deformation bands observed optically (see Fig. 10). (d) More equant recrystallized grains with well-defined grain boundary triple junctions, tj, that are characteristic of the shear zone core. (e) A recrystallized grain developed by progressive misorientation of dislocation networks to form new grain boundary. Continued intracrystalline deformation of the grain by dislocation, d, is characteristic of syndeformational rotation recrystallization. (f) Recrystallized grains from high-strain core of shear zone. Grain boundaries and triple junctions, tj, do not typically exhibit voids or tubules, in contrast to SZA.

with the absence of microstructures indicative of very high stresses that are observed near low-temperature faults (Kennedy and Logan, 1998; Kennedy and White, 2002) where extensive micro-twinning occurs in micrite-sized grains.

For all the distributions of recrystallized grain sizes from different areas (Fig. 6), there are distinct concentrations in the 5–10 μm range. Applying the empirical relationship of Rutter (1995) for rotation recrystallization gives stress estimates of 100 and 215 MPa for Type A and B shear zones, respectively. Notably, the temperature dependence of this relationship indicates that these equilibrium grain sizes form at temperatures on the order of 200 °C within the lower range of temperature estimates (Fig. 3). Paleostress estimates from both twins and recrystallized grain size are internally consistent in that the lower limit in on the order of 80–100 MPa, and the upper limit is about 200 MPa. These estimates do not preclude deformation at lower stresses for which there are no microstructural markers.

A deformation mechanism map for 250 °C has been constructed (Fig. 13a) to examine the implications of the various flow laws and to explore their consequences for interpretation of the observed microstructures. This is considered a liberal estimate of the maximum deformation temperature, with evidence from temperature studies (Table 1), deformation mechanisms (Covey-Crump, 1994) and recrystallization microstructures (Rutter, 1995) that deformation occurred between 200 and 250 °C.

5.3.3. Correlation of natural deformation and predicted rheological response

Flow laws describing the rheological response, themselves combinations of microphysical processes such as dislocation glide and climb, will contribute to the deformation rate independent of whether they are the dominant operative flow mechanism. The invocation of composite flow laws (White, 1980, 1982; Herwegh et al., 2005b; Vitale et al., 2007) is thus necessary to fully encompass the rock behaviour. The latter have to date been developed in most detail for calcite by Herwegh et al. (2005b).

Strain rate–stress curves (Fig. 13a) have been calculated for the initial (undeformed micrite) and final (deformed micrite and deformed vein calcite) grain size distributions using the flow laws of Walker et al. (1990). These relationships are preferred because the starting material for this study compares closely in grain size to the Portoro micrite and the grain size paleopiezometer used (Rutter, 1995) has been calibrated with these data. For the GSI (Eq. (4)) and GSS (Eq. (5)) relationships, a uniform stress condition is applied (Herwegh et al., 2005b). The strain rate for each flow law is determined according to

$$\dot{\epsilon} = \sum_i \dot{\epsilon}_i v_i \tag{8}$$

For a particular grain size class *i*, defined in increments of 2.5 m (Fig. 6), the strain rate $\dot{\epsilon}_i$ is determined, factored against its

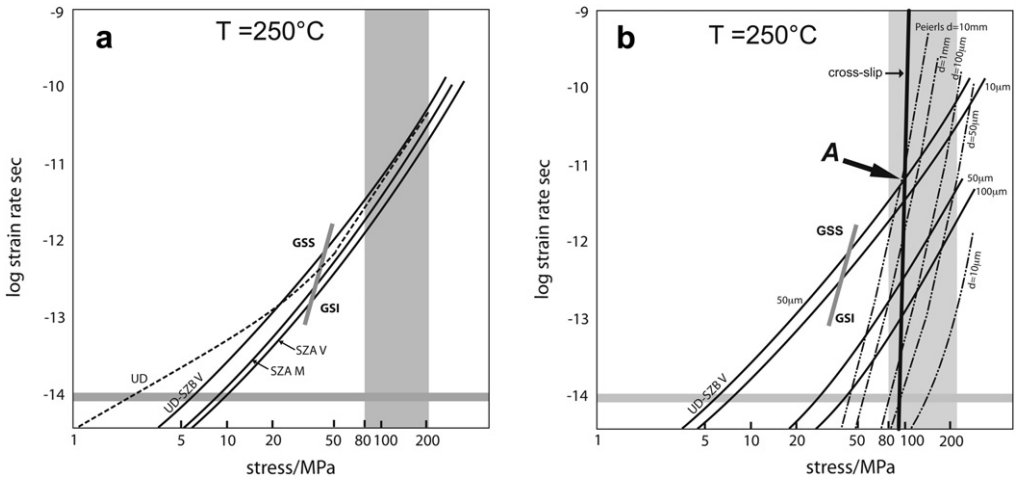

Fig. 13. Stress-strain rate maps constructed for calcite deformation at 250 °C. (a) Dashed line UD – composite flow law curve for diffusion creep (Herwegh et al., 2003) plus GSI creep (Walker et al., 1990) using the grain size distribution for undeformed micrite. Solid lines – composite flow law curves for GSS plus GSI creep after Walker et al. (1990) using grain size distributions from the noted samples. UD, undeformed micrite; SZA M, SZA deformed micrite; SZA V, SZA deformed vein calcite; SZB V, SZB deformed vein calcite. The boundary between grain-size-sensitive (GSS) and grain-size-insensitive (GSI) regimes for the calculated curves is shown. Stress estimates (80–215 MPa) are constrained by the shaded box. Additional details in text. (b) Comparison of micrite and recrystallized vein calcite behaviour. UD, SZA V as for Fig. 13a. Solid lines – GSI + GSS flow (Walker et al., 1990) for the grain size indicated. Heavy solid line – cross-slip (de Bresser, 2002). Dashed lines – Peierls law flow for grain size indicated. A – approximate equality point for competing flow laws. Additional details in text.

population fraction v_i and then summed over all the size classes. The strain rates for GSI and GSS relationships are then summed to produce the curves in Fig. 13a. For comparison, the strain rate–-stress curve was determined for the GSS diffusion-accommodated flow law, Eq. (7), using the undeformed micrite grain size distribution, and as above, combined with Eq. (5) to determine the composite strain rate.

Figure 13a enables construction of a plausible rheological history of the Portoro limestone shear zones as observed in their finite strain state. Assuming a history during which stress or imposed displacement rates increased during nappe formation, both diffusion- and dislocation-accommodated GSS mechanisms (Fig. 13a, curves UD and UD-SZB) would dominate deformation up to stresses of 40–50 MPa giving strain rates of 10^{-14} s^{-1}–10^{-12} s^{-1}. For both the micrite and vein calcite, estimated peak stresses indicate deformation within the GSI regime, a prerequisite for dynamic recrystallization of the veins. For a peak stress range of 80–200 MPa, the inferred strain rates are 10^{-12} s^{-1} for SZA deformed micrite and vein calcite, and 6×10^{-11} s^{-1} for SZB calc-mylonite, within the expected behaviour of narrow shear zones (Sibson, 1977; White and Mawer, 1986; Herwegh et al., 2005b; Vitale et al., 2007).

5.4. Why localization?

Despite the plausibility of the rheological response depicted by Fig. 13a, the spatial heterogeneity of deformation remains unexplained. If, as determined in Fig. 13a, the protolith is sufficiently weak to enable pervasive deformation at low differential stress, why do some micritic layers develop shear zones (Type A) and other exhibit unaffected primary sedimentary features? Likewise, why do some dolomite-bounded layers develop shear zones (Type B), and others none?

An explanation for heterogeneous nucleation of Type A shear zones may simply lie in variations of porosity/permeability associated with channelized fluid flux (section 5.2.3). There is certainly a dynamic component to the control of fluids, as only Type A shear zones are geochemically altered, raising the issue of whether fluid flow initiated deformation or vice versa. The occurrence of SZA within packages of similar shear zones would be consistent with an overall moderate to high strength response (rapid stress rise?) in the micrite, but with sufficient spatial variations in permeability and fluid flow to preferentially initiate more rapid displacement in certain layers that then control subsequent localization.

Type B shear zone calc-mylonites are fundamentally related to pre-existing veins. As noted, there is an orientation control on their localization by both the bedding-parallel mechanical anisotropy (boundary conditions), and the development of brittle (hydraulic) fractures within which the calcite veins formed; however, shear zones do not occur parallel to all bedding layers. Calcite veins commonly act as softening materials within low-temperature shear and fault zones (Kennedy and White, 2002). Macroscopic ductile localization requires sustained strain softening (Hobbs et al., 1990) of the vein calcite relative to its host.

The mechanisms by which the observed microstructures might develop are examined in Fig. 13b. Stress–strain rate curves for cross-slip (GSI), Peierls law flow for 10 mm vein calcite grains (see Fig. 10) and GSI flow of the primary micrite have a mutual intersection (Fig. 13b, Point A) at about 85–90 MPa, the lower limit of the paleostress estimates, giving a strain rate of 7×10^{-12} s^{-1}; for higher stresses, both the cross-slip and Peierls law relationships give faster strain rates for vein calcite (i.e. expend more power) than is ascribed to the micrite. Hence, the lower bound of stresses estimated for the main deformation corresponds closely to the stress at which veins would exhibit strain softening relative to the micrite. The absence of micrite deformation adjacent to Type B shear zones suggests that stress rises quickly enough that no evidence of lower strain rates is retained and/or ambient stress is sustained at magnitudes high enough to support glide-controlled processes, at the expense of GSI micrite deformation.

Dynamic recrystallization of the vein calcite is rapid relative to shear strain (Fig. 10b). The reduced grain size will, for Peierls law flow, create a Hall-Petch like hardening effect requiring an increasing stress to maintain a given strain rate. For an imposed displacement rate that generates stresses in the 100 MPa range, any small fluctuation to higher stress will favour the glide-controlled processes, particularly cross-slip that will affect all grains independent of size. The strong stress dependence predicts extreme strain rates at stresses well below the estimated maximum of 200 MPa. The latter response would be characteristic of run away shear, and, if operative, may form a ductile transition to fracture

(more veins?) if stress levels are not relaxed by dissipation of work in the shear zones.

The Peierls law description has comparable strength to cross-slip in the coarsest grains, but recrystallization would generate grain fractions requiring higher flow stresses for an imposed displacement rate (Fig. 13b). If Eq. (4) describes an appropriate flow law, such an increase in stress would also enable the vein material to remain 'softer' than the micrite. Concomitant with the microstructural evolution is the increasing contribution to strain rate within the vein material by the weak grain-size dependent flow (Eq. (5)) used to describe micrite deformation. Thus, the hardening tendency of smaller grain size for Peierls law-accommodated deformation is countered by the softening effect of the inverse size dependence. The two flow laws, Eqs. (4) and (5) contribute equally for grain sizes of about 50 μm, with Peierls law flow becoming dramatically stronger at smaller grain sizes. At the upper stress estimate of 200 MPa, corresponding to recrystallized grain sizes of approximately 5 μm (essentially the UD-SZB V curve), the calculated strain rates of micrite and recrystallized calcite are the same; that is, stresses remain sufficient in the vein calcite (Hall-Petch hardening) to preclude preferential deformation of micrite, until the microstructure of the vein calcite has evolved to that of the micrite. The absence of evidence for stress much greater than 200 MPa suggests rapid recrystallization in the latter stages of grain size reduction such that the switch away from dislocation-mediated flow is suppressed. From this point, an equilibrium state develops whereby vein and micrite material deform contiguously, and cannot be differentiated optically, as expressed by the incorporation of the vein into the micrite of SZA. The progressive diminishment of strong glide-controlled deformation removes the need for continued grain size reduction, explaining the bound imposed by micrite grain size. Essentially, equilibrium occurs at a combined material-deformation mechanism regime boundary (e.g. de Bresser et al., 2001). In this end-state, both materials dissipate power equivalently for subsequent deformation at comparable conditions in the manner of Austin and Evans (2007).

From this study, Tuscan nappe formation entailed early development of stresses on the order of 100 MPa where there is an equivalency of strain rates among the micrite and vein calcite flow laws. This stress is necessarily less than the effective stress to induce brittle fracture (hydraulic fracture) of the type that formed the vein (Rowe and Rutter, 1990; Kennedy and White, 2002). At lower differential stress or imposed displacement rates, intracrystalline deformation and recrystallization would be less extensive; instead, vein calcite would appear as strong elements within deformed micrite where GSS dislocation- or diffusion-accommodated GBS would be the dominant process.

6. Conclusions

1. Calcite aggregates deformed naturally at 200–250 °C exhibit r$\{10\bar{1}4\}$ and f$\{01\bar{1}2\}$ glide dislocations in grains varying from 1 μm to 10 mm in size. The development of significant macroscopic intracrystalline strain is enabled by athermal network-accommodated recovery.
2. Dynamic recrystallization occurs by subgrain/cell rotation. Grain size reduction of vein calcite does not effectively surpass the initial grain size of the host micrite. This is explained by the micrite deforming near a mechanism regime boundary or by fortuitously having a grain size close to the equilibrium recrystallization size.
3. Paleostress estimates range from 80 to 215 MPa using both twins and recrystallized grain size. Associated strain rates are 10^{-12} s^{-1} and 6×10^{-11} s^{-1} for the end-state microstructures.
4. Consideration of dislocation glide-controlled flow laws (cross-slip and Peierls stress) demonstrates the strain softening attributes of coarse vein calcite at stresses on the order of 100 MPa. Interplay of grain-size hardening and grain size softening processes produce a scenario consistent with the minimum recrystallized grain size, and hence, maximum estimated stress.
5. Contrasting CPOs form in initially fine-grained and dynamically recrystallized calcite. The former reflects non-uniform deformation by fluid-enhanced GBS aided by a more 'permeable' grain boundary structure. The recrystallized calcite has 'tighter', low diffusivity grain boundaries that constrain deformation to be more uniform, giving a standard CPO.
6. Integration of EBSD patterns with microstructures and inferences about operative slip systems must be done carefully. Despite the good SPO and evidence of dislocation glide in the deformed micrite, no CPO formed. In the recrystallized vein calcite, the *c*-maximum suggests activity of basal glide, but only r- and f-type dislocations are observed to date.

Acknowledgements

Financial support by the University of Pisa (GM) and NSERC Canada Discovery grants (JCW and LAK) is acknowledged. The UNB Microscopy and Microanalysis Facility was established with support of the Canada Foundation for Innovation. S. Belfry, S. Cogswell, Dr. D. Hall and Dr. L. Weaver are thanked for their technical assistance. Reviews by H. de Bresser and an anonymous referee, and additional comments by B. LaFrance aided in clarifying several issues.

Appendix. Flow law parameters

T	temperature (K)
k	Boltzmann's constant
R	gas constant
σ	stress
$\dot{\epsilon}$	stress rate
d	grain size

Cross-slip (de Bresser, 2002)

log$K$	6.9 (material constant)
μ_0	3418 MPa (shear modulus)
μ	$\mu_0 - 9.7$ T (temperature-adjusted shear modulus)
b	6.37×10^{-10} m (Burgers vector)
α	2.18
γ	0.192 J m^{-2} (stacking fault energy)
ΔU_{cs}	$(\frac{\mu b^3}{1859(\gamma/\mu b)})(\ln[\frac{2\sqrt{3}}{16\pi(\gamma/\mu b)}])^{1/2}$

Peierls law flow (Renner et al., 2002)

A_P	3.16 M Pa^{-2} s^{-1}
Σ_P	78MPa kK^{-1}
K	115 M Pa kK^{-1} μm$^{1/2}$
T_m	1600 K (melting temperature)
Q_P	200 kJ/mol (activation energy)
σ_P	$(\Sigma_{P,0} + Kd^{-1/2})(T_M - T)$

GSI power law (Walker et al., 1990)

A_{GSI}	100 (material constant)
Q_{GSI}	190 kJ/mole (activation energy)
n	3.3 (stress exponent)
m	−1.3 (grain size exponent)

GSS dislocation-accommodated (Walker et al., 1990)

A_{GSS}	79433 (material constant)
Q_{GSS}	190 kJ/mole (activation energy)
n	1.7 (stress exponent)
m	−1.9 (grain size exponent)

GSS diffusion-accommodated flow (Herwegh et al., 2003)

A_D	4.266×10^6 (material constant)
Q_D	200 kJ/mole (activation energy)
n	1.1 (stress exponent)
m	−3.3 (grain size exponent)

References

Abbate, E., Balestrieri, M.L., Bigazzi, G., Norelli, P., Quercioli, C., 1994. Fission-track dating and recent rapid denudation in Northern Apennines, Italy. Memorie Società Geologica Italiana 48, 579–585.

Austin, N.J., Evans, B., 2007. Paleowattmeters: a scaling relation for dynamically recrystallized grain size. Geology 35, 343–346.

Badertscher, N.P., Burkhard, M., 2000. Brittle-ductile deformation in the Glarus thrust Lochseiten (LK) calc-mylonite. Terra Nova 12, 281–288.

Balestrieri, M.L., Bernet, M., Brandon, M.T., Picotti, V., Reiners, P., Zattin, M., 2003. Pliocene and Pleistocene exhumation and uplift of two key areas of the Northern Apennines. Quaternary International 101–102, 67–73.

Behrmann, J.H., Tanner, D.C., 2006. Structural synthesis of the Northern Calcareous Alps, TRANSALP segment. Tectonophysics 414, 225–240.

Bernet, M., Brandon, M.T., Garver, J.I., Molitor, B.R., 2004. Fundamentals of detrital zircon fission-track analysis for provenance and exhumation studies with examples from the European Alps. In: Bernet, M., Spiegel, C. (Eds.), Detrital Thermochronology; Provenance Analysis, Exhumation, and Landscape Evolution of Mountain Belts. Geological Society of America Special Paper 378, pp. 25–36.

Bernoulli, D., 2001. Mesozoic-Tertiary carbonate platforms, slopes and basins of the external Apeninnes and Sicily. In: Vai, G.B., Martini, P.I. (Eds.), Anatomy of an Orogen. Kluwer Academic Publishers, pp. 307–326.

de Bresser, J.H.P., 2002. On the mechanism of dislocation creep of calcite at high temperature: inferences from experimentally measured pressure sensitivity and strain rate sensitivity of flow stress. Journal of Geophysical Research 107, 2337. doi:10.1029/2002JB001812.

de Bresser, J.H.P., Spiers, C.J., 1993. Slip systems in calcite single crystals deformed at 300–800 °C. Journal of Geophysical Research 98, 6397–6409.

de Bresser, J.H.P., Peach, C.J., Reijs, J.P.J., Spiers, C.J., 1998. On dynamic recrystallization during solid state flow: effects of stress and temperature. Geophysical Research Letters 25, 3457–3460.

de Bresser, J.H.P., Ter Heege, J.H., Spiers, C.J., 2001. Grain size reduction by dynamic recrystallization: can it result in major rheological weakening? International Journal of Earth Sciences 90, 28–45.

de Bresser, J.H.P., Evans, B., Renner, J., 2002. Estimating the strength of calcite rocks under natural conditions. In: de Meer, S., Drury, M.R., de Bresser, J.H.P., Pennock, G. (Eds.), Deformation Mechanisms, Rheology and Tectonics: Current Status, Future Perspectives. Geological Society, London Special Publication, vol. 200, pp. 293–307.

Burkhard, M., 1990. Ductile deformation mechanisms in micritic limestones naturally deformed at low temperatures (150–350 °C). In: Knipe, R.J., Rutter, E.H. (Eds.), Deformation Mechanisms, Rheology and Tectonics. Geological Society, London, Special Publication, vol. 54, pp. 241–257.

Burkhard, M., 1992. Calcite twins, their geometry, appearance and significance as stress-strain markers and indicators of tectonic regime: a review. Journal of Structural Geology 20, 1–18.

Carmignani, L., Decandia, F.A., Disperati, L., Fantozzi, P.L., Lazzarotto, A., Liotta, D., Oggiano, G., 1995. Relationship between the Tertiary structural evolution of the Sardinia-Corsica-Provençal and the Northern Apennines. Terra Nova 7, 128–137.

Carosi, R., Leoni, L., Montomoli, C., Sartori, F., 2003. Very low-grade metamorphism in the Tuscan Nappe, Northern Apennines, Italy: relationships between deformation and metamorphic indicators in the La Spezia mega-fold. Schweizerische Mineralogische und Petrographische Mitteilungen 83, 15–32.

Carter, K.E., 1990. Construction and collapse of an orogen: strain and fluid history of the Tuscan Nappe, Northern Apennines, Italy. Ph.D. thesis, University of Texas at Austin.

Carter, K.E., 1992. Evolution of stacked shear zones in carbonates from mid-crustal levels: Tuscan Nappe, Northern Apennines, Italy. Journal of Structural Geology 14, 182–192.

Carter, K.E., Dworkin, S.I., 1990. Channelized fluid flow through shear zones during fluid-assisted dynamic recrystallization, Northern Appenines, Italy. Geology 15, 720–723.

Carter, K.E., Mosher, S., 1987. Apeninne Thrusting and Post-Appenine Gravity Sliding in the Portovenere Area, N. Apennines, Italy. In: Geological Society of America Abstracts with Program, vol. 19, 613 pp.

Cerrina Feroni, A.G., Plesi, G., Fanelli, G., Leoni, L., Martinelli, P., 1983. Contributo alla conoscenza dei processi metamorfici di grado molto basso (anchi-metamorfismo) a caricco della falda toscana nell'area del ricoprimento apuano. Bolletino Società Geologica Italiana 102, 269–280.

Cerrina Feroni, A., Martelli, L., Martinelli, P., Ottria, G., Catanzariti, R., 2002. Carta Geologico-Strutturale Dell'Appennino Emiliano-Romagnolo-Note Illustrative. Regione Emilia-Romagna. Selca Firenze.

Ciarapica, G., Passeri, L., 1980. La litostratigrafia della Serie Triassica del Promontorio Occidentale del Golfo della Spezia. Memorie Società Geologica Italiana 21, 51–61.

Covey-Crump, S.J., 1994. The application of Hart's state variable description of inelastic deformation to Carrara marble at $T < 450$°C. Journal of Geophysical Research 99, 19793–19808.

Ebert, A., Herwegh, M., Pfiffner, A., 2007a. Cooling induced strain localization in carbonate mylonites within a large-scale shear zone (Glarus thrust, Switzerland). Journal of Structural Geology 29, 1164–1184.

Ebert, A., Herwegh, M., Berger, A., Pfiffner, A., 2007b. Grain coarsening maps for polymineralic carbonate mylonites: a calibration based on data from different Helvetic nappes (Switzerland). Tectonophysics 457, 128–142.

Ebert, A., Herwegh, M., Evans, B., Pfiffner, A., Austin, N., Vennemann, T., 2007c. Microfabrics in carbonate mylonites along a large-scale shear zone (Helvetic Alps). Tectonophysics 444, 1–26.

Elter, P., 1960. I lineamenti tettonici dell' evolutivi dell'Appennino a Nord-Ovest delle Apuane. Bollettino Della Società Geologica Italiana 79, 273–312.

Elter, P., 1975. Introduction à la géologie de l'Apennin septentrional. Bulletin Société Géologique France 7, 956–962.

Federici, P.R., Raggi, G., 1976. Una nuova interpretazione della tettonica dei Monti della Spezia. Bollettino Della Società Geologica Italiana 94, 945–960.

Fellin, M.G., Reiners, P.W., Brandon, M.T., Wuthrich, E., Balestrieri, M.L., Molli, G., 2007. Thermochronologic evidence for exhumational history of the Alpi Apuane metamorphic core complex, northern Apennines, Italy. Tectonics 26, TC6015. doi:10.1029/2006TC002085.

Gianmarino, S., Giglia, G., 1990. Gli elementi strutturali della piega di La Spezia nel contesto geodinamico dell'Appennino Settentrionale. Bollettino Società Geologica Italiana 109, 683–692.

Gifkins, R.C., 1976. Grain-boundary sliding and its accommodation during creep and superplasticity. Metallurgical Transactions 7A, 1225–1232.

Guillopé, M., Poirier, J.-P., 1979. Dynamic recrystallization during creep of single crystal halite: an experimental study. Journal of Geophysical Research 84, 5557–5567.

Herwegh, M., Ebert, A., 2009. Grain-scale Interplay of Deformation Mechanisms and Fluid Flow and the Implication for Large-scale Shear Zones. In: Geophysical Research Abstracts 11, pp. EGU 2009–2686.

Herwegh, M., Kunze, K., 2002. The influence of nano-scale second-phase particles on deformation of fine grained calcite mylonites. Journal of Structural Geology 24, 1463–1478.

Herwegh, M., Pfiffner, O.A., 2005. Tectono-metamorphic evolution of a nappe stack: a case study of the Swiss Alps. Tectonophysics 404, 55–76.

Herwegh, M., Xiao, X., Evans, B., 2003. The effect of dissolved magnesium on diffusion creep in calcite. Earth and Planetary Science Letters 212, 457–470.

Herwegh, M., Berger, A., Ebert, A., 2005a. Grain coarsening maps: a new tool to predict microfabric evolution of polymineralic rocks. Geology 33 (10), 801–804.

Herwegh, M., de Bresser, J.H.P., ter Heege, J.H., 2005b. Combining natural microstructures with composite flow laws: an improved approach for the extrapolation of lab data to nature. Journal of Structural Geology 27, 503–521.

Hirth, G., Tullis, J., 1992. Dislocation creep regimes in quartz aggregates. Journal of Structural Geology 14, 145–159.

Hobbs, B.E., Mulhaus, H.B., Ord, A., 1990. Instability, softening and localization of deformation. In: Knipe, R.J., Rutter, E.H. (Eds.), Deformation Mechanisms, Rheology and Tectonics. Geological Society, London, Special Publication, vol. 54, pp. 71–80.

Iannace, A., Vitale, S., 2004. Ductile shear zones in carbonates: the calcaires plaquettés of northern Calabria (Italy). Comptes Rendus Geosciences 336, 227–234.

Kennedy, L., Logan, J.M., 1997. The role of veining and dissolution in the evolution of fine-grained mylonites – the McConnell thrust. Journal of Structural Geology 19, 785–797.

Kennedy, L., Logan, J.M., 1998. Microstructures of cataclasites in a limestone-on-shale thrust fault: implications for low-temperature recrystallization of calcite. Tectonophysics 295, 167–186.

Kennedy, L.A., White, J.C., 2002. Low temperature recrystallization of calcite: mechanisms and consequences. Geology 29, 1027–1030.

Kirschner, D.L., Kennedy, L., 2001. Limited syntectonic fluid flow in carbonate-hosted thrust faults of the Front Ranges, Canadian Rockies, inferred from stable isotope data and structures. Journal of Geophysical Research 106, 8827–8840.

Kocks, U.F., Argon, A.S., Ashby, M.F., 1975. Thermodynamics and kinetics of slip. Progress in Materials Science 19, 1–288.

Lickorish, W.H., Henry, W., Butler, R.W.H., 1996. Fold amplification and parasequence stacking patterns in syntectonic shoreface carbonates. Geological Society of America Bulletin 108, 966–977.

Linzer, H.-G., Ratschbacher, L., Frisch, W., 1995. Transpressional collision structures in the upper crust; the fold-thrust belt of the Northern Calcareous Alps. Tectonophysics 242, 41–61.

Mainprice, D.H., Paterson, M.S., 1984. Experimental studies of the role of water in the plasticity of quartzites. Journal of Geophysical Research 89, 4257–4269.

Mancktelow, N.S., Pennacchioni, G., 2004. The influence of grain boundary fluids on the microstructure of quartz-feldspar mylonites. Journal of Structural Geology 26, 47–69.

Mancktelow, N.S., Gruijic, D., Johnson, E.L., 1998. An SEM study of porosity and grain boundary microstructure in quartz mylonites. Contributions to Mineralogy and Petrology 131, 1–85.

McLaren, A.C., 1986. Some speculations on the nature of high-angle grain boundaries in quartz rocks. In: Hobbs, B.E., Heard, H.C. (Eds.), Mineral and Rock Deformation; Laboratory Studies; the Paterson Volume. Geophysical Monograph 36, pp. 233–245.
McQuarrie, N., 2004. Crustal scale geometry of the Zagros fold-thrust belt, Iran. Journal of Structural Geology 26, 519–535.
Miller, J., 1988. Multistage dolomitization of the Portoro Limestone, Liguria, Italy. M.A. thesis, University of Texas, Austin, Texas.
Miller, J.K., Folk, R.L., 1994. Petrographic, Geochemical and Structural Constraints on the Timing and Distribution of Postlithification Dolomite in the Rhaetian Limestone ('Calcare Nero') of the Portovenere Area, La Spezia, Italy. In: International Association of Sedimentologists Special Publication, vol. 21, pp. 187–202.
Mistler, R.E., Coble, R.L., 1974. Grain-boundary diffusion and boundary widths in metals and ceramics. Journal of Applied Physics 45, 1507–1509.
Molli, G., 2008. Northern Apennine-Corsica orogenic system: an updated review. In: Siegesmund, S., Fügenschuh, B., Froidzheim, N. (Eds.), Tectonic Aspects of the Alpine-Dinaride-Carpathian System. Geological Society, London Special Publications, vol. 298, pp. 413–442.
Molli, G., Vaselli, L., 2006. Structures, interference patterns and strain regime during mid-crustal deformation in the Alpi Apuane (Northern Apennines, Italy). In: Mazzoli, S., Butler, R. (Eds.), Styles of Continental Contraction. Geological Society of America Special Paper 424, pp. 79–93.
Montomoli, C., 2002. Vein development and fluid inclusion data: insight on the evolution of the Tuscan Nappe in the Northern Appenines. Bolletino Società Geologica Italiana Volume Speciale 1, 801–817.
Montomoli, C., Ruggieri, G., Boiron, M.C., Cathelineau, M., 2001. Pressure fluctuation during uplift of the Northern Appenines (Italy): a fluid inclusions study. Tectonophysics 341, 121–139.
Panozzo Heilbronner, R., 1992. The autocorrelation function: an image processing tool for fabric analysis. Tectonophysics 212, 351–370.
Pennock, G.M., Coleman, M., Drury, M.R., Randle, V., 2009. Grain boundary plane populations in minerals; the example of wet NaCl after low strain deformation. Contributions to Mineralogy and Petrology 158, 53–67.
Ramsay, J.G., 1967. Folding and Fracturing of Rocks. McGraw-Hill, New York, 568 pp.
Renner, J., Evans, B., Siddiq, G., 2002. Dislocation creep of calcite. Journal of Geophysical Research 107, 2364. doi:10.1029/2001JB001680.
Reutter, K.J., Teichmuller, M., Teichmuller, R., Zanaucchi, G., 1978. Coalification studies in the Northern Apeninnes and paleogeothermal implications. In: Closs, H., Roeder, D., Schmidt, K. (Eds.), Alps, Apennines and Hellenides. Schweizerbart'sche Verlagbuchhandlung, Stuttgart, pp. 261–267.
Rowe, K.J., Rutter, E.H., 1990. Paleostress estimation using calcite twinning: experimental calibration and application to nature. Journal of Structural Geology 12, 1–17.
Rutter, E.H., 1974. The influence of temperature, strain rate and interstitial water in the experimental deformation of calcite rocks. Tectonophysics 22, 311–334.
Rutter, E.H., 1995. Experimental study of the influence of stress, temperature and strain on the dynamic recrystallization of marble. Journal of Geophysical Research 100, 24651–24663.
Rutter, E.H., 1999. On the relationship between the formation of shear zones and the form of the flow law for rocks undergoing dynamic recrystallization. Tectonophysics 303, 147–158.
Schmid, S.M., 1975. The Glarus overthrust: field evidence and mechanical modal. Eclogae Geologicae Helvetiae 68, 247–280.
Schmid, S.M., 1976. Rheological evidence for changes in the deformation mechanism of Solnhofen limestone toward low stresses. Tectonophysics 31, T21–T28.
Schmid, S.M., Boland, J.N., Paterson, M.S., 1977. Superplastic flow in finegrained limestone. Tectonophysics 43, 257–259.
Schmid, S.M., Paterson, M.S., Boland, J.N., 1980. High temperature flow and dynamic recrystallization in Cararra marble. Tectonophysics 65, 245–280.
Sibson, R.H., 1977. Fault rocks and fault mechanisms. Journal of the Geological Society, London 133, 191–193.
Spratt, D.A., Dixon, J.M., Beattie, E.T., 2004. Changes in structural style controlled by lithofacies contrast across transverse carbonate bank margins; Canadian Rocky Mountains and scaled physical models. American Association of Petroleum Geologists Memoir 82, 259–275.
Stipp, M., Tullis, J., 2003. The recrystallized grain size piezometer for quartz. Geophysical Research Letters 30, 2088. doi:10.1029/2003GL018444.
Storti, F., 1995. Tectonics of Punta Bianca promontory: Insights for the evolution of the Northern Apennines-Northern Tyrrhenian sea basin. Tectonics 14, 832–847.
Taini, V., 2003. Strutture e processi di deformazione di bassa temperatura in rocce carbonatiche: esempio della falda toscana nella zona di La Spezia. Thesis, University of Pisa.
Teixell, A., Durney, D.W., Arboleya, M.-L., 2000. Stress and fluid control on décollement within competent limestone. Journal of Structural Geology 22, 349–372.
Thomas, D.B., Nance, R.D., Murphy, J.B., 2002. Deformation of the Macumber formation, Antigonish basin, Nova Scotia; implications for the Ainslie detachment. Atlantic Geology 38, 135–144.
Turner, F.J., 1953. Nature and dynamic interpretation of deformation in calcite of three marbles. American Journal of Science 251, 276–298.
Turner, F.J., Griggs, D.T., Heard, H.C., 1954. Experimental deformation of calcite crystals. Geological Society of America Bulletin 65, 883–933.
Twiss, R.J., 1977. Theory and applicability of a recrystallized grain size palaeopiezometer. Pure and Applied Geophysics 115, 227–244. doi:10.1007/BF01637105.
Ulrich, S., Schulmann, K., Casey, M., 2002. Microstructural evolution and rheological behaviour of marbles deformed at different crustal levels. Journal of Structural Geology 24, 979–995.
Urai, J.L., Means, W.D., Lister, G.S., 1986. Dynamic recrystallization of minerals. In: Hobbs, B.E., Heard, H.C. (Eds.), Mineral and Rock Deformation: Laboratory Studies. American Geophysical Union Geophysical Monograph 36, pp. 161–199.
Vitale, S., White, J.C., Iannace, A., Mazzoli, S., 2007. Ductile strain partitioning in micritic limestones, Calabria, Italy: the roles and mechanisms of intracrystalline and intercrystalline deformation. Canadian Journal of Earth Sciences 44, 1587–1602.
Walker, A.N., Rutter, E.H., Brodie, K.H., 1990. Experimental study of grain-size sensitive flow of synthetic, hot pressed calcite rocks. In: Knipe, R.J., Rutter, E.H. (Eds.), Deformation Mechanisms, Rheology and Tectonics. Geological Society, London, Special Publication, vol. 54, pp. 259–284.
Wenk, H.-R., 1985. Carbonates. In: Wenk, H.-R. (Ed.), Preferred Orientations in Deformed Metals and Rocks: An Introduction to Modern Texture Analysis. Academic, San Francisco, CA, pp. 361–384.
White, J.C., 1980. A study of deformation within the Flinton Group conglomerates, southeastern Ontario. Ph.D. thesis, University of Western Ontario, London, Canada.
White, J.C., 1982. Quartz deformation and the recognition of recrystallization regimes in the Flinton Group conglomerates, Ontario. Canadian Journal of Earth Sciences 19, 81–93.
White, J.C., Mawer, C.K., 1986. Extreme ductility of feldspars from a mylonite, Parry Sound, Canada. Journal of Structural Geology 8, 133–143.
White, J.C., White, S.H., 1980. A high voltage electron microscope study of naturally deformed dolomite. Tectonophysics 66, 35–54.
White, J.C., White, S.H., 1981. The structure of grain boundaries in tectonites. Tectonophysics 78, 613–628.
Zattin, M., Picotti, V., Zuffa, G.G., 2002. Fission-track reconstruction of the front of the Northern Apennine thrust wedge and overlying Liurian Unit. American Journal of Science 302, 346–379.